The
ENGINEERS' DIGEST

REVIEW OF ENGINEERING PROGRESS ABROAD

VOL. VI. No. 9 SEPTEMBER, 1945

NOV 2 1945
ENGINEERING LIBRARY

Churchill
PRECISION GRINDING MACHINES
GRINDING FROM THE SOLID ECCENTRIC
FINS ON AERO ENGINE CYLINDERS
USING A MULTI-RIBBED WHEEL
There is a CHURCHILL machine for
every precision grinding job.
THE CHURCHILL MACHINE TOOL CO., LTD., MANCHESTER.
HOME SELLING AGENTS . . . . . CHARLES CHURCHILL & CO. LTD. (BIRMINGHAM & BRANCHES)
EXPORT SALES ORGANISATION . . ASSOCIATED BRITISH MACHINE TOOL MAKERS Ltd. (London & Branches)

THE ENGINEERS' DIGEST

REVIEW OF ENGINEERING PROGRESS ABROAD

Published Monthly at 120, Wigmore Street, London, W. 1.

Publishers : **ENGINEERS' DIGEST LTD.** – – – – – – – Telephone : WELBECK 9357

Advertisement Dept. – 120, Wigmore Street, London, W.1. – – Telephone : WELBECK 9357

Distribution – – E. & F. N. SPON, LTD., 57, Haymarket, London, S.W.1.
Telephone : Whitehall 1860. Telegrams : Fenspon, Lesquare, London

Editorial Dept. – – 120, Wigmore Street, London, W.1. – – Telephone : WELBECK 9357

Subscriptions to : ENGINEERS' DIGEST LTD., 120, Wigmore Street, London, W.1, or
E. & F. N. SPON, LTD., 57, Haymarket, London, S.W.1.

ANNUAL SUBSCRIPTION OF 12 NUMBERS, £2 2s. **SINGLE COPIES, 4s. 6d.**

ADVISORY COMMITTEE

J. F. ALCOCK, B.A., A.M.I.Mech.E.
R. W. ALLOTT, M.A., A.R.Ae.S.
E. ALTON, D.Eng., A.M.Inst.B.E.
H. H. ASBRIDGE, M.B.E., M.I.Mech.E.
R. W. AYERS, M.I.W.
Co L. J. BOWDEN, M.Inst.C.E., M.I.Mech.E.
H. H. BROUGHTON, M.I.Mech.E.
F. BUCKINGHAM, B.Sc., A.M.Inst.C.E., A.M.I.Mech.E.,
T. H. BURNHAM, B.Sc. (Lond.), A.M.I.Mech.E. [A.M.I.E.E.
J. S. CASWELL, M.Sc., M.I.Mech.E.
G. C. SAFFERY COOPER.
J. DICK, Ph.D., B.Sc., A.M.I.Mech.E.
D. FIFE, M.I.Mech.E.
G. E. FOXWELL, D.Sc. (Lond.), F.Inst.P., F.Inst.F.,
R. GRIFFITHS, M.Sc. [M.Inst.Gas.E.
H. HEYWOOD, Ph.D., M.Sc. (Eng.), A.M.I.Mech.E.
O. HURST, M.Inst.N.A.
Capt. J. S. IRVING, M.I.Mech.E., M.I.A.E., A.F.R.Ae.S., M.S.A.E.
F. C. JOHANSEN, M.Sc. (Eng.), M.I.Mech.E., F.R.Ae.S., M.I.Loco.E.
W. J. KEARTON, D.Eng., M.I.Mech.E., A.M.Inst.N.A.
Prof. W. KERR, Ph.D., M.I.Mech.E.
G. V. LOMONOSOFF, Dr.Ing., M.I.Mech.E.
B. J. LYMER, M.I.Mech.E.
D. T. MacIVOR, M.I.Mech.E., M.Cons.E.
W. O. MANNING, F.R.Ae.S.
R. B. MATTHEWS, Wh.Ex., A.M.Inst.C.E., M.I.E.E., F.R.Ae.S.
Prof. A. L. MELLANBY, D.Sc., LL.D., M.I.Mech.E.
J. H. R. RATCLIFFE, B.Sc. (Eng., Hons.), M.I.Mech.E.
Col. C. W. D. ROWE.
W. A. SCOBLE, D.Sc., A.R.C.Sc., M.I.Mech.E.
P. W. SEEWER, D.E. (Zurich), M.Inst.C.E., M.I.Mech.E.
Prof. S. PARKER SMITH, D.Sc., M.I.E.E., A.M.Inst.C.E.
C. F. H. VERITY, A.M.Inst.C.E., A.M.I.E.E., A.M.I.Mech.E.
E. G. WALKER, F.C.G.I., B.Sc. (Eng.), M.Inst.C.E., M.I.Mech.E., M.Am.Soc.C.E.
Major F. L. WATSON, M.Inst.C.E., M.I.Mech.E.
G. WATSON, M.Inst.C.E., M.I.Mech.E.
C. H. WOODFIELD, M.I.Mech.E., M.I.Struct.E.
T. WRIGHT, Ph.D., M.Sc.
M. L. YATES, Ph.D., M.Sc.Tech., M.A. (Com.), M.I.Mech.E.

"Cronite"
REGD. TRADE MARK
The HIGH TEMPERATURE ALLOY
SALT, LEAD AND CYANIDE VESSELS
CARBURIZING BOXES AND POTS
ROTARY RETORTS & PROPELLING WORMS
FURNACE HEARTHS AND FITTINGS
ENAMELLING PERRITS AND SUPPORTS
GLASS-BLOWING NOZZLES
PYROMETER PROTECTION SHEATHS
CASTINGS FOR USE AT 700°/1200° C.
The CRONITE FOUNDRY Co. LTD
LAWRENCE RD · TOTTENHAM · LONDON N.15
PHONE · STAMFORD HILL 4237

CONTENTS

page

Application of X-Ray Analysis of Metallurgical Problems 245
" *The Engineers' Digest*," *Vol.* 6, *No.* 9, *p.* 245.

Chrome Plating increases Life of Forge Dies 247
" *The Engineers' Digest*," *Vol.* 6, *No.* 9, *p.* 247.

Device for Measuring the Angle of Twist of Shafts revolving at High Speeds 241
" *The Engineers' Digest*," *Vol.* 6, *No.* 9, *p.* 241.

Graphical Method for the Analysis of Gas-Dynamic Problems 225
" *The Engineers' Digest*," *Vol.* 6, *No.* 9, *p.* 225.

Properties of High Temperature Alloy Steels 243
" *The Engineers' Digest*," *Vol.* 6, *No.* 9, *p.* 243.

Radial and Lateral Reactions acting upon the Wheels of a Motor Car 235
" *The Engineers' Digest*," *Vol.* 6, *No.* 9, *p.* 235.

Some Applications of Hydraulic Motors 248
" *The Engineers' Digest*," *Vol.* 6, *No.* 9, *p.* 248.

Take-off of Heavily Loaded Aircraft by Means of Towing Aircraft 231
" *The Engineers' Digest*," *Vol.* 6, *No.* 9, *p.* 231.

The Application of the Combustion Turbine to the Propulsion of Ships 240
" *The Engineers' Digest*," *Vol.* 6, *No.* 9, *p.* 240.

Beauty - accuracy - high finish

are characteristics of modern plastics

The manufacture of plastics is a mass-production business but is nevertheless a craft. The skill of the craftsman who once patiently shaped and carved and polished each product of his hands has been replaced by the skill of the tool-designer and the toolmaker creating the beauty, accuracy and finish of modern plastics.

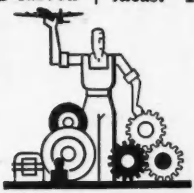

That is why our service* employs the best designers and toolmakers to interpret our customers' ideas. Their work ensures that we can produce large quantities of rubber and plastic mouldings accurately, economically and quickly.

Well-designed and well-made tools are cheapest in the end.

★ *Manufacture of Products in Plastics, Rubber and Synthetic Rubbers*

LORIVAL PLASTICS

UNITED EBONITE & LORIVAL LTD · LITTLE LEVER · NEAR BOLTON

TELEPHONE: FARNWORTH 676 (FOUR LINES) · TELEGRAMS: 'EBONITE' LITTLE LEVER

U E L

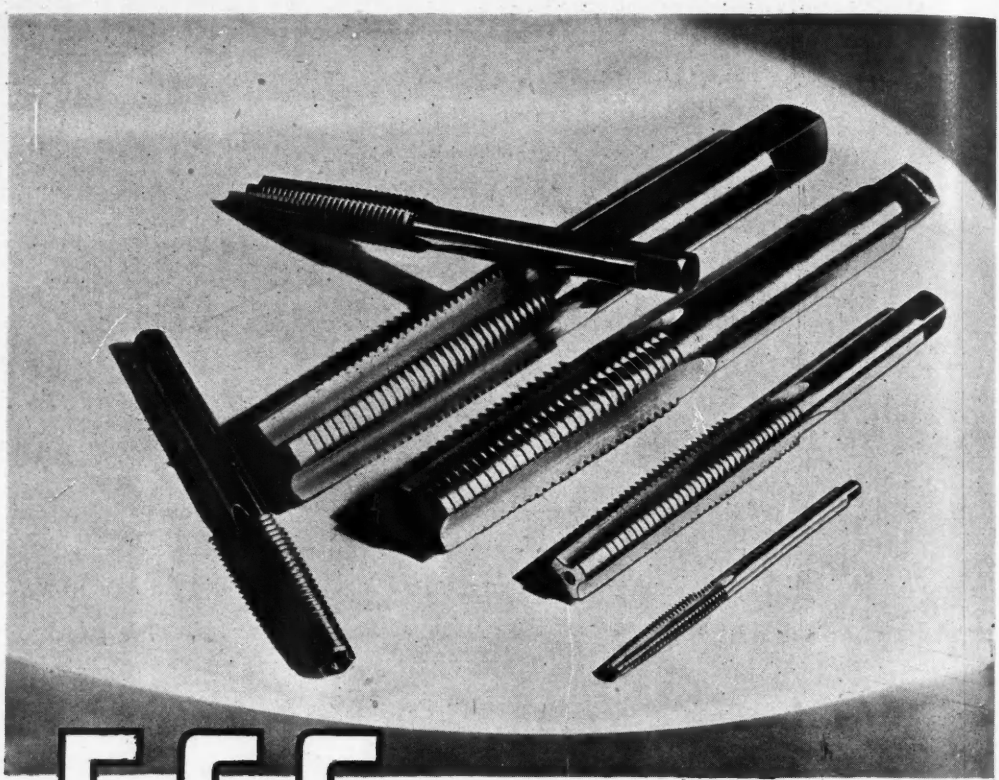

ESC GROUND THREAD TAPS

Conform to the provisions of British Standard Specifications 949/1941.

With our modern plant and equipment, we make Ground Thread Taps, Chasers, etc., of an accuracy of pitch and refinement of form unobtainable with cut form thread tools. Complete Range of Ground Thread Taps in production, most of which can be delivered from Stock.

ENGLISH STEEL CORPORATION LTD

OPENSHAW MANCHESTER

GRAPHICAL METHOD FOR THE ANALYSIS OF GAS-DYNAMIC PROBLEMS.

By P. DE HALLER. (From *Technische Rundschau Sulzer*, No. 1, 1945, pp. 6-24).

PRESENT day trends in the design of reciprocating prime movers are characterised by the employment of steadily increasing engine speeds and working pressures. It is an inherent feature of reciprocator operation at high speed that masses of gases required to be periodically accelerated with greatest rapidity, hereby causing the occurrence of pressure and velocity waves within the body of the gas. Thus, for instance, in internal combustion engines, the rapid outflow of gas during the exhaust period leads to a waste of pressure energy because of the incurrence of turbulence, pressure oscillations, and heat generation by fluid friction. It goes without saying that considerations of highest overall efficiency demand that such losses should be kept to a minimum.

Determination of the required cross-sectional areas of the exhaust ports and exhaust pipes on the basis of quasi-stationary flow proves inadmissible because of the rapidity with which the exhaust process takes place. Nor is it possible to analyse the flow phenomena occurring in radial or axial blowers by having recourse to the ordinary concepts of aerodynamics, because these concepts can take account only of slight variations in the density of the gas. This objection applies equally well to the flow phenomena met with in induction and exhaust pipes of internal combustion engines. The experimental method does not provide any solution to this problem as far too many imponderable factors are present. The only way open to gauge the magnitude of the losses involved therefore is the employment of the analytical methods of gas dynamics.

A simple and sufficiently accurate graphical method for the analysis of the phenomena involved in two-dimensional stationary flow at supersonic velocity was suggested by Prandtl and Busemann. As this method is based upon the general properties of partial differential equations of the hyperbolic type it can be applied in a more general form to problems that admit a solution on the basis of this type of equation.

The application of this method to the investigation of the non-stationary flow of a gas in a round pipe is particularly simple ; and no difficulties are met with in applying this method to the solution of more complex problems such as supersonic flow in axial-symmetrical configurations, or non-stationary flow in a pipe of varying cross-section. The actual application of this method to a given problem usually is made with the use of a Légendre transformation or of Riemann's theory of the integration of partial differential equations. These mathematical concepts, however, are little known to engineers, thus barring the way to the full understanding of the work done in this field. Drawing upon the earlier fundamental work of Hugoniot, a more direct and more easily understandable method is outlined below. An additional advantage of this type of approach is that this method is better adapted to the usual practice followed in graphical solutions.

APPLICATION TO LINEAR NON-STATIONARY FLOW.

The adiabatic flow of a gas within a thermally-insulated cylinder is defined by

$$\frac{\partial \rho}{\partial t} + u\frac{\partial \rho}{\partial x} + \rho\frac{\partial u}{\partial x} = 0 \quad .. \quad .. \quad (1)$$

and

$$\frac{\partial u}{\partial t} + u\frac{\partial u}{\partial x} + \frac{1}{\rho}\frac{\partial \rho}{\partial x} = 0 \quad .. \quad .. \quad (2)$$

where u is the velocity of the gas flowing in the direction x coincident with the longitudinal axis of the pipe ; p is the pressure, and ρ is the density of the gas, and t is the time. By introducing the velocity potential ϕ (with $u = \frac{\partial \phi}{\partial x}$ and considering that p is a function of ρ, we have

$$\frac{\partial^2 \phi}{\partial x \partial t} + \frac{\partial \phi}{\partial x}\frac{\partial^2 \phi}{\partial x} + \frac{a^2}{\rho}\frac{\partial \rho}{\partial x} = 0 \quad .. \quad (3)$$

where $a = \sqrt{\frac{\partial p}{\partial \rho}}$ is the velocity of sound.

We integrate and obtain the Bernoulli equation in its general form

$$\frac{\partial \phi}{\partial t} + \frac{1}{2}\left(\frac{\partial \phi}{\partial x}\right)^2 = -\int_{\rho_0}^{\rho} \frac{a^2}{\rho}\, d\rho = -f(\rho) \quad .. \quad (4)$$

assuming the arbitrary time function to be zero. By solving equations (3) and (4) for $\frac{\partial \rho}{\partial x}$ and $\frac{\partial \rho}{\partial t}$ respectively, and introducing the expressions obtained into equation (1) we have

$$\frac{\partial^2 \phi}{\partial t^2} + 2\frac{\partial \phi}{\partial x}\cdot\frac{\partial^2 \phi}{\partial x\, \partial t} + \left(\left(\frac{\partial \phi}{\partial x}\right)^2 - a^2\right)\frac{\partial^2 \phi}{\partial x^2} = 0 \quad (5)$$

For the sake of greater simplicity, the partial derivatives of x and t may be denoted

$$\left(\phi_x = \frac{\partial \phi}{\partial x}\,;\ \phi_t = \frac{\partial \phi}{\partial t}\right) \text{ and so on.}$$

It is well known that differential equations generally do not have an analytical solution which satisfies both the equation and the boundary conditions. The solution must therefore be obtained by finding partial solutions by the finite increment method. Geometrically a solution is represented by a plane, and it must be ascertained under what conditions a curve will be tangent with two integral planes. A curve of this type is called characteristic. If ϕ' and ϕ'' be the two solutions, the following equations will then apply to the characteristic, to wit :—

$$(\phi'_{tt} - \phi''_{tt}) + 2\,\phi_x\,(\phi'_{xt} - \phi''_{xt}) + (\phi_x^2 - a^2)\,(\phi'_{xx} - \phi''_{xx}) = 0$$

$$d\,(\phi'_x - \phi''_x) = dt\,(\phi'_{xt} - \phi''_{xt}) + (\phi'_{xx} - \phi''_{xx}) = 0$$

$$d\,(\phi'_t - \phi''_t) = (\phi'_{tt} - \phi''_{tt})\,dt + dx\,(\phi'_{xt} - \phi''_{xt}) = 0$$

These are three linear homogeneous equations for $(\phi'_{xx} - \phi''_{xx})$ and as these differences are $\neq 0$ if $\phi' \neq \phi''$, the determinant of the system must be

$$\begin{vmatrix} 1 & 2\phi_x & (\phi^2_x - a^2) \\ 0 & dt & dx \\ dt & dx & 0 \end{vmatrix} = dx^2 - 2\,\phi_x\,dx\,dt + (\phi^2_x - a^2)\,dt^2$$

$$= (dx - (\phi_x + a)\,dt)$$

$$(dx - (\phi_x - a)\,dt) = 0$$

and

$$\frac{dx}{dt} = \phi_x \pm a. \quad .. \quad .. \quad .. \quad (6)$$

This equation represents the differential equation of the projections of the characteristics upon the (x, t) plane. We therefore have *two* families of curves with the directional coefficients

$$\frac{dx}{dt} = \phi_x + a \quad (6a) \qquad \text{and} \qquad \frac{dx}{dt} = \phi_x - a \quad (6b)$$

The range of validity of each singular solution is delimited by two characteristics of each family of cha-

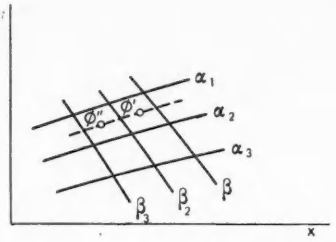

Fig. 1. **Range of validity of a solution in the characteristics diagram.**

racteristics (Fig. 1). The variations in ϕ_x and ϕ_t along a characteristic is

$$d\,\phi_x = \phi_{xt}\,dt + \phi_{xx}\,dx$$

With the use of equation (6) it therefore becomes:

$$\frac{d\phi_x}{dt} = \phi_{xt} + (\phi_x \pm a)\,\phi_{xx}$$

and

$$\frac{d\phi_t}{dt} = \phi_{tt} + (\phi_x \pm a)\,\phi_{xt}$$

By multiplying by $-(\phi \pm a)$ and (-1) respectively, and totalling up, it obtains:

$$-(\phi \pm a)\frac{d\phi_x}{dt} - \frac{d\phi_t}{dt} = (a^2 - \phi_x^2)\,\phi_{xx} - 2\,\phi_x\,\phi_{xt} - \phi_{tt} = 0$$

$$d\,\phi_t = -(\phi_x \pm a)\,d\,\phi_x \quad .. \quad .. \quad (7)$$

which represents two families of curves in the (ϕ_x, ϕ_t) plane, a curve of (7) being coordinate with each characteristic, and *vice versa*.

By expressing ϕ_t by ϕ_x and by ρ according to equation (4) and substituting $d\phi_t = -\frac{df}{d\rho}\,d\rho - \phi_x\,d\phi_x$ in equation (7) it becomes

$$d\phi_x \pm \frac{1}{a}\frac{df}{d\rho}\,d\rho = 0 \quad .. \quad .. \quad (8)$$

By integration it then follows:

$$\phi_x = \mp \int \frac{a}{\rho}\,d\rho$$

This constitutes a relationship between the density and the velocity of the gas along a characteristic. In the case of adiabatic changes of state of an ideal gas, the velocity of sound is related with the density by the expression

$$a = \sqrt{\frac{dp}{d\rho}} = a_o \left(\frac{\rho}{\rho_o}\right)^{\frac{\kappa-1}{2}} \quad \text{where } \kappa = \frac{c_p}{c_v} \text{ is the ratio of the specific heat at constant pressure to that at constant volume. The factors } a_o \text{ and } \rho_o \text{ apply to the state of rest of the gas. It then is:}$$

$$\int \frac{a}{\rho}\,d\rho = \frac{2}{\kappa-1}\,a$$

so that the equations (8) will take the form

$$du = -\frac{2}{\kappa-1}\,da \quad (9a) \qquad \text{and} \qquad du = \frac{2}{\kappa-1}\,da \quad (9b)$$

By integration:

$$u_2 - u_1 = \mp \frac{2}{\kappa-1}(a_2 - a_1) \quad .. \quad (9)$$

This equation expresses the functionality between the velocity of flow and the sound velocity along a characteristic. As the pressure p is defined by the velocity of sound according to the relationship $\frac{p}{p_o} = \left(\frac{a}{a_o}\right)^{\frac{2\kappa}{\kappa-1}}$, the equation (9) therefore indicates the pressure variation coordinated with a given variation in velocity.

The equations (6) and (9) may be used for establishing a graphical method of analysis which corresponds exactly with that developed by Prandtl and Busemann. The new method consists in charting the networks of the mutually coordinated characteristics in a location diagram (t, x) and a condition diagram (a, u) as shown in Figs. 2 and 3. If a and u are given for two points 1 and 3 of the location diagram, the points 1′ and 3′ in the condition diagram will also be determined, and the characteristics passing through 1′ and 3′ can be drawn according to equation (9) hereby also defining the points 2′ and 4′. The portions 1 — 3 and 3 — 4, etc., of the characteristics are approximately represented by straight lines the slope of which corresponds to that existing at the midway points of 1′4′, 3′4′, etc. The points of intersection of these straight lines will then determine the points 2 and 4. In this way the entire network of characteristics of the location diagram may be plotted on the basis of the boundary conditions.

It will be found convenient to introduce dimensionless values by dividing by suitable reference dimensions such as the pipe length L and the velocity of sound a_0 prevailing in the state of rest. By making

$$A = \frac{a}{a_o}; \quad X = \frac{x}{L}; \quad U = \frac{u}{a_o}; \quad Z = \frac{a_o}{L}\,t$$

the basic equations (6) and (9) will take the form

$$\frac{dX}{dZ} = U \pm A\,dU = \mp \frac{2}{\kappa-1}\,dA$$

By making the A scale $\frac{2}{\kappa-1}$ times larger than the U

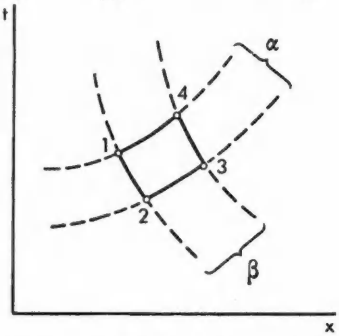

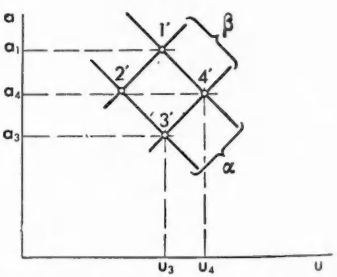

Figs. 2 and 3. **Interrelationship between the characteristics in the location diagram (t, x) and in the condition diagram (a, u).**

scale, the characteristics of the condition diagram will be straight lines with a slope of 45 deg. relative to the axes of the system. This procedure will be found to greatly simplify the actual construction of the diagram. By means of the straight lines $U = A$ and $U = -A$ the slope $\frac{dX}{dZ}$ of the straight-line portions of the location diagram characteristics will be easily obtained. If $\overline{Z}$, $\overline{U}$, and $\overline{X}$ represent the lengths of the dimension-less units in cm., all that is required is to draw the vertically upward-directed line $P'H' = P''H'' = \frac{\overline{Z}\,\overline{U}}{\overline{X}}$ in points P' and P'' (Fig. 4). These lines will then possess the required direction.

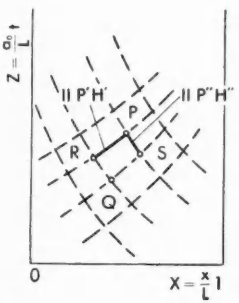

As $i = \frac{a^2}{\kappa - 1}$, the equation $i_e = i + \frac{u^2}{2}$ can be written $a_e^2 = a^2 - \frac{\kappa - 1}{2} u^2$ where i_e and a_e denote enthalpy and velocity of sound respectively in the external space during conditions of rest. In this case the loci representing the conditions prevailing at the pipe outlet will be found to lie on an ellipse in the (a, u) diagram (Fig. 5).

So far it was assumed that an identical state of rest of the gas prevails in the entire pipe. Cases are frequently met with in practice in which a body of gas at one temperature pushes another body of gas at different temperature ahead of it, so that different velocities of sound are coordinate with identical pressures. The graphical method permits to compute the partial reflections which a wave undergoes at the interface, as well

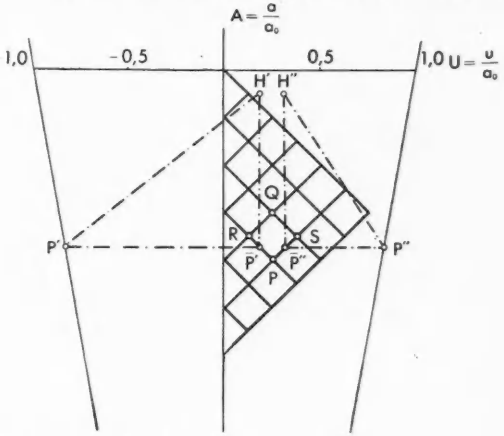

Fig. 4. Step by step construction of the location and condition diagrams.

BOUNDARY CONDITIONS.

The boundary conditions obtaining at the ends of the pipe will largely depend upon the kind of problem considered. If, for instance, the cylinder is closed by means of a piston, the movement of which is determined by a known law, the velocity of the gas layer abounding the piston will equal the velocity u_0 of the piston. Another case frequently encountered in practice is that of a pipe leading to atmosphere, or to a large vessel the internal pressure of which may be taken as constant. The pressure prevailing in the outlet section of the pipe must not *a priori* be assumed to be identical with the external pressure, but account must be taken of the fact that the fluctuating discharge is the source of pressure waves. These pressure waves will determine the pressure to be introduced into the boundary conditions prevailing at the outlet section.

In a method like the present one, which in the main is intended for the use by engineers, it would be difficult to make allowance for this effect. The pressure in the outlet section will therefore be assumed to be equal to the external pressure, provided the velocity of discharge s below the velocity of sound. The loci representing this type of discharge will therefore be found upon the horizontal straight line coordinate with the external pressure p_e and the straight line $A = U$ or $a = u$ (Fig. 5).

In the case of a reversal of flow it must be considered that in this event the pressure at the pipe outlet will be below the atmospheric pressure, and the Bernoulli equation must be established accordingly.

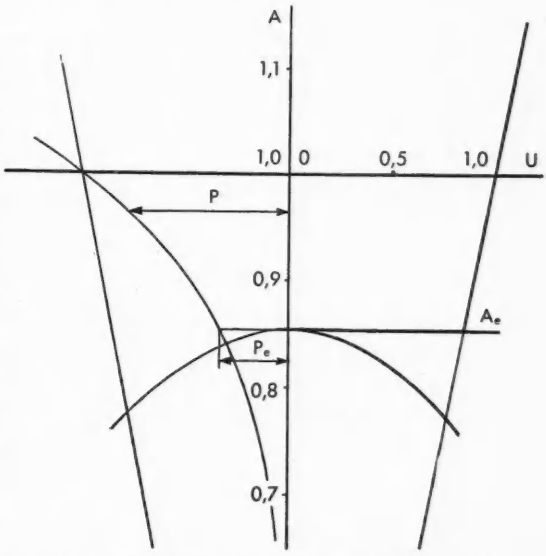

Fig. 5. Boundary condition in the condition diagram for constant pressure during admission and exhaust.

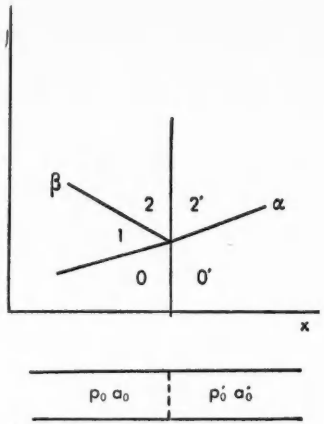

Fig. 6. **Sudden change in initial condition (temperature jump).**

as the changes which take place upon passage of the wave through the interface (Figs. 6 and 7). In order to simplify matters the interfacial boundary layer may be assumed to be of infinite thinness, the diffusion effect being ignored. Obviously the interface will travel along the pipe at the velocity of flow of the gases proper. If $p_o a_o$ and $p_o' a_o'$ denote the respective initial conditions of the two gas bodies, corresponding condition diagrams (a, u) and (a', u') may be charted. At the interface the following conditions must then be satisfied, to wit :

$$u = u' \text{ and } p = p', \text{ where } p = p_o \left(\frac{a}{a_o}\right)^{\frac{2\kappa}{\kappa-1}} \text{ and}$$

$$p' = p_o' \left(\frac{a'}{a_o'}\right)^{\frac{2\kappa}{\kappa-1}}$$

By choosing the scales for a and a' in such a manner that their units are in the proportion $\frac{p_o^{\frac{\kappa-1}{2\kappa}}}{p_o'} \frac{a_o'}{a_o}$, identical curves $p = f(a)$ and $p' = f'(a)$ will result, and any two loci having the same coordinates will therefore satisfy the boundary conditions. Both diagrams can thus be combined in one single chart. Furthermore, by selecting the scales for a and u in such a way that the characteristics include angles of 45 deg. with the axes of the system, the characteristics in the $(a' u')$ diagram will then have a slope given by

$$\tan \gamma = \pm \frac{a_o}{a_o'} \left(\frac{p_o'}{p_o}\right)^{\frac{\kappa-1}{2\kappa}}$$

In all other respects, the graphical solution of the problem remains the same as that outlined above. Referring to Fig. 7 it is easily seen that passage of a wave from the one temperature region to the other is accompanied by a partial reflection.

The diagrams given in Figs. 8a and 8b refer to the flow conditions prevailing in a pipe of constant cross section, the one end of the pipe $(X = 0)$ being connected to a vessel of constant internal pressure p, while the other end $(X = 1)$ connects with atmosphere. The end $(X = 1)$ remains closed for $t < 0$ and is suddenly opened at time $t = 0$. Because of this unsteady initial condition the point (1, 0) in the (X, Z) diagram must be a singular point. With the point is coordinated the part of the characteristic (α) passing through (0, 1), this part being delimited by the point (0, 1) and the point of intersection with the straight line $U = A$.

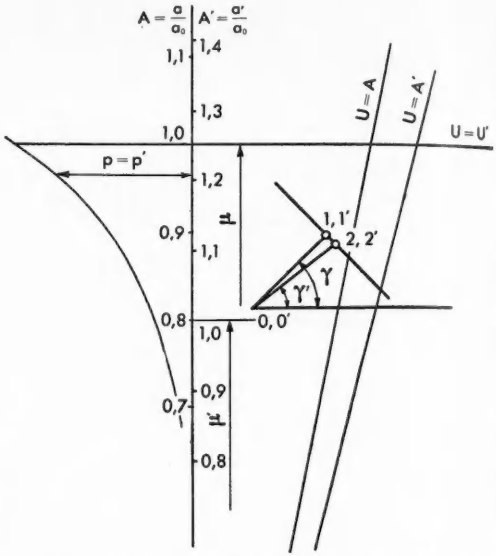

Fig. 7. **Condition diagram incorporating temperature jump.**

An infinite number of characteristics (β) will therefore originate in point (1, 0) of the location diagram, the expansion waves travelling along these characteristics and towards the end $(X = 0)$ of the pipe. These waves, upon being reflected at the end of the pipe, will return in the form of compression waves to the point of origin $(X = 1)$ from whence they will be reflected again, and so forth. The speed of propagation of the primary expansion waves will remain constant as long as they do not meet with any reflected waves. The characteristics (β) originating at point $(X = 1, Z = 0)$ will therefore at first be straight lines. The latter are represented in the condition diagram by point situated on the characteristic

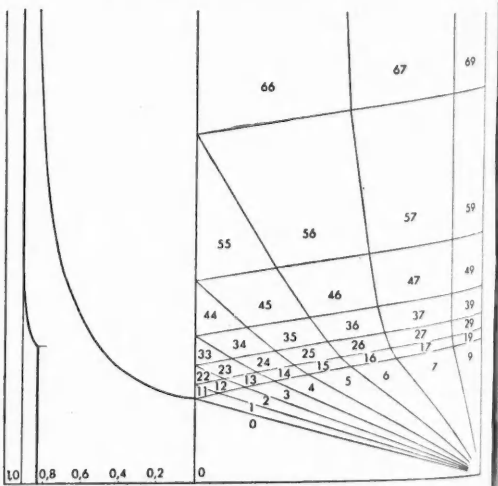

Fig. 8a. **Flow conditions in pipe.** Location diagram.

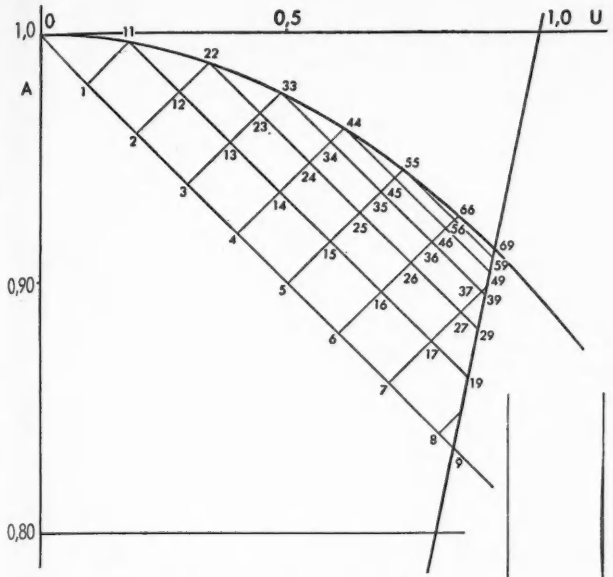

Fig. 8b. **Flow conditions in pipe.** Condition diagram.

(α) which passes through point (0, 1). But whenever the primary waves meet with reflected waves, their speed of propagation will cease to be constant, and the characteristics (β) will take the shape of curves in the location diagram, these curves being coordinated with the characteristics (β) (1, 11), (2, 22), etc., as shown in the condition diagram. The loci of the conditions resulting from the reflections 11, 22, 33, etc., therefore will lie upon the ellipse defined by Bernoulli's equation.

The diagram given in Fig. 9 refers to the analytical investigation of the pressure waves existing in the exhaust pipe of a four stroke cycle internal combustion engine. In this case a cylinder of constant volume is evacuated into a straight cylindrical pipe, the movement of the exhaust valve following a given law. The free end of the pipe is seen to be provided with a nozzle (turbine nozzle). The initial pressure prevailing in the cylinder is p_o, while p'_o is the atmospheric pressure prevailing in the exhaust pipe prior to the opening of the exhaust valve. The expansion of the gas in the cylinder may be adiabatic and the ratio $\frac{p_o}{p'_o}$ may be such that the gas velocity in the valve area equals the velocity of sound when expansion commences. In this case the rate of flow of the gas exhausted solely is a function of the valve aperture and the cylinder pressure. It therefore is a known function of time from which function the gas velocity at the pipe inlet can be computed. Note should, however, be taken of the fact that the velocity of flow in the pipe is below the velocity of sound, while the gas leaves the valve at supersonic speed.

The non-adiabatic transition which takes place can be computed as follows:

It is $$F\rho\, u = F_1\rho_1\, u_1 = $$
$$= F_1\rho_o\, a_o \left(\frac{2}{\kappa+1}\right)^{\frac{\kappa+1}{2(\kappa-1)}}$$

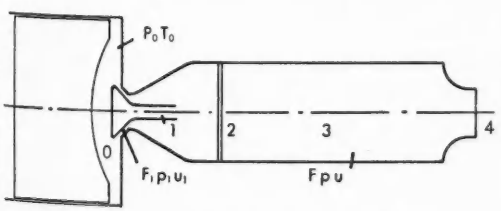

Fig. 9. **Diagram for computation of pressure waves in exhaust pipe of four stroke cycle engine.**
0 = cylinder; 1 = valve; 2 = compression wave impulse; 3 = exhaust line; 4 = turbine nozzle.

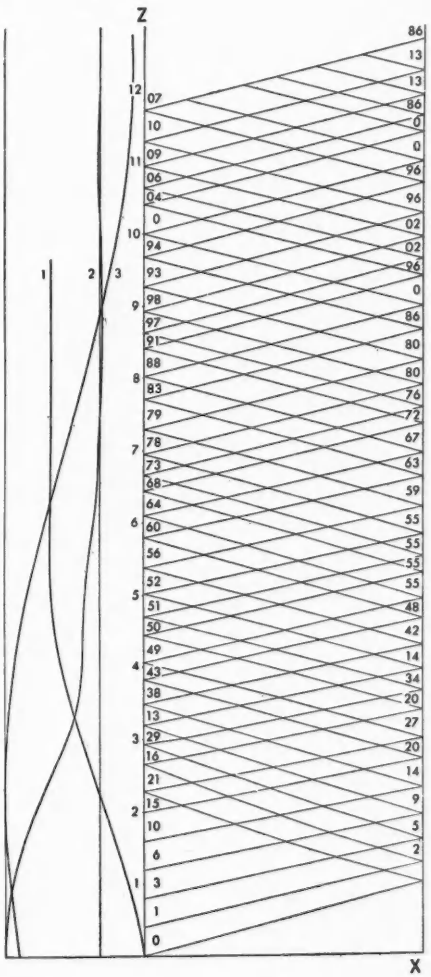

Fig. 10a. **Location diagram of pressure waves in exhaust pipe of four stroke cycle engine.**
(1) Valve diagram (2) Pressure in cylinder (3) Piston travel.

$$a_0^2 - a^2 = \frac{\kappa-1}{2} \cdot u^2$$

$$a_0^2 - a_1^2 = \frac{\kappa-1}{2} \cdot u_1^2$$

$$u_1^2 = a_1^2 = \frac{2}{\kappa+1} a_0^2$$

so that

$$F \cdot p \frac{u}{u_0} = F_1 p_0 \left(\frac{2}{\kappa+1}\right)^{\frac{\kappa+1}{2(\kappa-1)}} \cdot \left(1 - \frac{\kappa-1}{2} \cdot \frac{u^2}{a_0^2}\right)$$

in which only p is unknown.

The second equation available is that of the characteristic which reads

$$u - u' = \pm \frac{2}{\kappa-1} (a - a') =$$

$$= \frac{2}{\kappa-1} a_0' \left[\left(\frac{p}{p'_0}\right)^{\frac{\kappa-1}{2\kappa}} - \left(\frac{p'}{p'_0}\right)^{\frac{\kappa-1}{2\kappa}}\right]$$

where p'_0 and a'_0 are the initial pressure and the initial velocity of sound respectively in the pipe, while u' and a' characterise the conditions in the pipe prior to a variation in the valve aperture F. By solving these two equations the boundary conditions existing at the inlet of the pipe can then be found. The initial value of a'_0 of course will vary over the length of the pipe, but for the sake of simplification a constant average value of a'_0 was used in this instance. The location and condition characteristics obtained in this manner are given in Figs. 10a and 10b. In Figs. 11a and 11b the analytical result is compared with the results of a test made on a six cylinder engine with the use of a piezoelectric indicator. The discrepancy displayed between theoretical and actual values in the later stages of the process is due to the fact that the theoretical results were arrived at without regard to the influence of the exhaust connections of the other cylinders nor to that of the scavenging air.

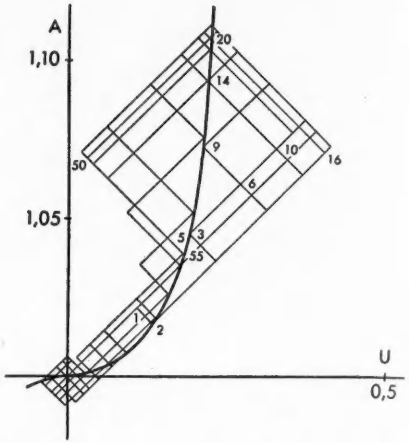

Fig. 10b. **Condition diagram of pressure waves in exhaust pipe of four stroke cycle engine.**

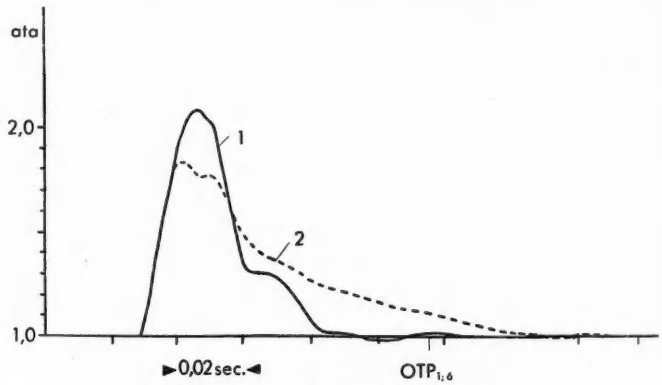

Fig. 11a. **Pressure diagram (at turbine inlet).**
1 = computed ; 2 = measured.

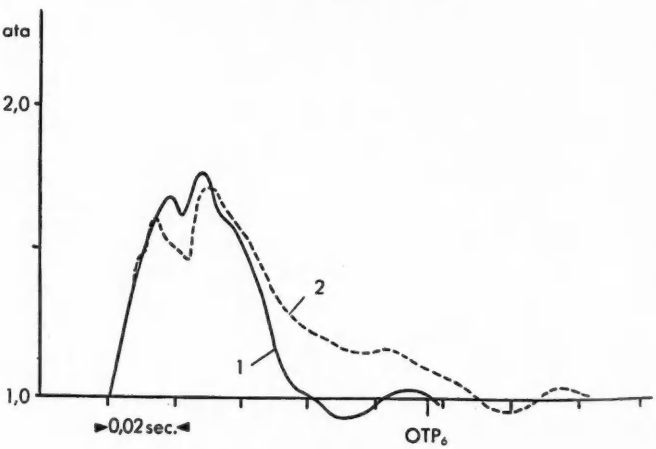

Fig. 11b. **Pressure diagram (at cylinder).**
1 = computed ; 2 = measured.

TAKE-OFF OF HEAVILY LOADED AIRCRAFT BY MEANS OF TOWING AIRCRAFT*.

By K. URECH. (From *Flug-Wehr und Technik*, No. 9, Sept., 1944, pp. 258-260, and No. 10, Oct. 1944, pp. 283-288).

A. General.

AT present, the dimensions of the airport are not, as of old, determined by the length of the landing run but by the length of the take-off run. This change has been brought about by the development of landing aids, such as wheel brakes, landing flaps, and quite recently the braking propeller. When landing, the weight of fuel carried has decreased considerably, while at take-off the wing loading is highest. Thus, in spite of small improvements easing take-off, the length of take-off run to that of the landing run is about 3 to 1.

In the following article it will be shown that by employing towing aircraft for assisted take-off, the take-off run can be considerably shortened.

BASIC EQUATIONS FOR TAKE-OFF.

The process of take-off can be subdivided into three groups characterised by :

(a) length of roll S_R
(b) speed at unsticking v_{ab}
(c) length of climb S_h (up to clearing an obstacle of given height, generally $h = 20$ m.).

(*a*) *Length of roll.*

The equation of motion can be written

$$\frac{G}{g} \cdot \frac{dv}{dt} = S - \mu \cdot G - q \cdot F_{tr} \cdot (c_w - \mu \cdot c_a) \quad .. \quad (1)$$

where G = take-off weight (kg.)
S = propeller thrust (kg.)
F_{tr} = wing area (m²)
g = acceleration due to gravity (m./sec.²) = 9.81 ;
q = dynamic pressure (kg./m²)
c_a, c_w = lift coefficient and drag coefficient variable with α, the angle of incidence during rolling
$\frac{dv}{dt}$ = acceleration.

The accelerating force is then,

$$K = S - \mu \cdot G - q\, F_{tr} \cdot (c_w - \mu\, c_a) \quad .. \quad (2)$$

i.e., K is a function of the speed v.

The solution of the differential equation (1) can easily be obtained by graphical integration over the whole range $v=0$ to $v=v_{ab}$. This method enables one to account for any variation of the values S, q, μ and α (and thus c_a and c_w). Equation (1) offers two possible ways of calculation according to the transformation chosen :

(*aa*) Direct integration of the length of roll in case of interest for a final result only ; one can write in eq. (1) :

$$\frac{dv}{dt} = \frac{dv}{ds} \cdot \frac{ds}{dt} = \frac{dv}{ds} \cdot v \quad .. \quad .. \quad (3)$$

and after substituting of further values,

$$ds_r = M \frac{v}{K} dv \quad .. \quad (4) \qquad K = f(v)\, M = \frac{G}{g} \frac{dv}{dt}$$

$$s_r = M \int_0^v \frac{v}{K} \cdot dv \quad .. \quad .. \quad (5)$$

By plotting $M \cdot \frac{v}{K}$ against v and integrating the so obtained curve graphically, s_r can be plotted as

$$s_r = f(v_{ab}) \quad .. \quad .. \quad .. \quad (6)$$

(*bb*) The second method consists of two integrations, one giving for each speed v the required time t, the other the length of the landing run travelled, s_r. This solution is based directly on equation (1) :

$$dt = \frac{M}{K(v)} \cdot dv \quad .. \quad .. \quad .. \quad (7)$$

$$t_r = \int_0^v \frac{M}{K} \cdot dv \quad .. \quad .. \quad .. \quad (8)$$

By plotting $\frac{M}{K}$ against v, and integrating the resulting curve, $t_r = f(v)$ for every value of v is obtained. This curve is valuable for various take-off problems, especially for test purposes. In turning the co-ordinate system, from curve $t_r = f(v)$ the relation $v = f(t)$ is obtained, and with

$$ds = v \cdot dt \quad .. \quad .. \quad (9)$$

a second integration yields $s_r = f(t)$:

$$s_r = \int_0^t v \cdot dt \quad .. \quad .. \quad .. \quad (10)$$

The so found $s_r = f(t)$ can be represented as a function of v by means of a simple graphical construction (Fig. 1). Draw through point A of curve $s(t)$ parallels to the co-ordinate axes $\overline{AE}$ and $\overline{AD}$. $\overline{AE}$ intersects the previously drawn curve $t(v)$ at point B. Extend line $\overline{AD}$ until it intersects the 45 deg.-axis through the origin O at point C. A parallel line to the abscissa through point C intersects the extension of line $\overline{FB}$ at A', which is a point of the curve $s_r(v)$ corresponding to point A of curve $s(t)$. Proof : $A'F = CD = AE = s$ because of the intersection with the 45 deg.-axis, and $EB = OF$ is the speed v corresponding to time $t = OE$.

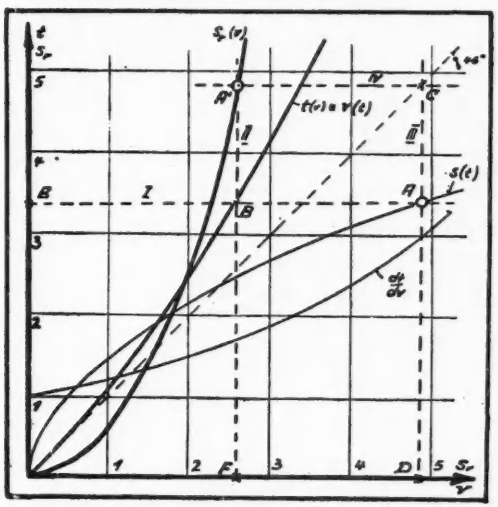

Fig 1

*The present paper is based on the Dissertation of the Author and of R. Kassowitz in the Federal Technical College, Zurich. The problem was raised by Prof. Dr. T. Ackeret.

If the knowledge of t at every instant is not required, the aforementioned tedious double integration can be avoided and a speedy solution obtained by the following reasoning. We have

$$s_r = \bar{v} \cdot t_{ab} \quad .. \quad .. \quad .. \quad (11)$$

where $\bar{v} = \dfrac{v_0 + v_{ab}}{2} = \dfrac{1}{2} v_{ab}$, and t_{ab} = total time required until unsticking. There can be obtained from curve $\dfrac{M}{K}$ by means of equations (7) and (8):

$$t_{ab} = \int_0^{v_{ab}} \frac{M}{K} \cdot dv \quad .. \quad .. \quad (8a)$$

t_{ab} corresponds to area *ODEF* in Fig. 2, and the mean value $\bar{v}$ is also rapidly found. According to Mises, $\bar{v}$ is the distance from the ordinate of the centroid of area *ODEF*. From equations (10) and (11)

$$\bar{v} = \frac{s_r}{t_{ab}} = \frac{\int_0^{t_{ab}} v \cdot dt}{t_{ab}}$$

Now, E_1 the static moment of the area $OAJF$ about the axis $\overline{AJ}$ (Fig. 2) is equal to E_2, the static moment of $ADEJ$ about the same axis. Thus,

$$E_1 - E_2 = \int_0^{\bar{v}} (\bar{v} - v)\, m \cdot dv - \int_{\bar{v}}^{v_{ab}} (v - \bar{v})\, m \cdot dv = 0$$

wherein $m = \dfrac{M}{K} = \dfrac{dt}{dv}$.

A condition can be established which is identical to the above, however it is simpler to give the proof in determining the distance a of the centroid of area *ODEF* from the ordinate.

Thus, we have

$$a = \frac{\textit{static moment of area ODEF about ordinate}}{\textit{area ODEF}}$$

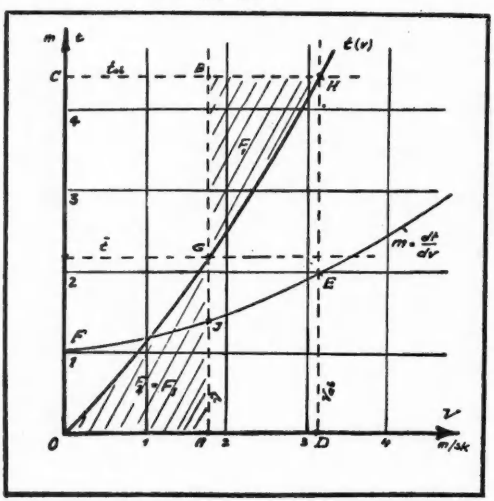

Fig. 2

Substituting the required expressions

$$a = \frac{\int_0^{v_{ab}} m \cdot dv \cdot v}{\int_0^{v_{ab}} m \cdot dv} = \frac{v_{ab} \cdot t_{ab} - \int_0^{v_{ab}} t \cdot dv}{t_{ab}}$$

According to Fig. 2 the numerator of the right hand expression is equal to area $OHC = \int_0^{ab} v \cdot dt = s_r$; and therefore $a = \dfrac{s_r}{t_{ab}}$ which proves that $a = \bar{v}$.

All that is needed for practical purposes is to find area *ODEF*, say by planimeter. This equals t_{ab}, and the distance of the centroid of area *ODEF* from the ordinate is $\bar{v}$. Then, $s_r = \bar{v} \cdot t_{ab}$.

(*b*) *Speed at unsticking.*

The speed at unsticking v_{ab} is obtained from the equilibrium condition, lift A equals weight G:

$$A = c_a \cdot q \cdot F_{tr} = G \quad .. \quad .. \quad (12)$$

Therefore

$$v_{ab} = \sqrt{\frac{G}{F_{tr}} \cdot \frac{2}{\rho} \cdot \frac{1}{c_a}} \quad .. \quad .. \quad (13)$$

(*c*) *Length of climb.*

If φ is the angle of inclination of the flight path from the horizontal, the equilibrium condition of stationary climb perpendicular to the flight path is expressed by

$$A = G \cos \varphi \quad .. \quad .. \quad .. \quad (14)$$

and in direction of flight by

$$S - W = G \sin \varphi \quad .. \quad .. \quad (15)$$

From equation (15)

$$\sin \varphi = \frac{S - W}{G},$$

and the horizontal distance s_h to clear an obstacle of given height h is

$$s_h = h \operatorname{cotan} \varphi \quad .. \quad .. \quad .. \quad (16)$$

B. Unassisted Take-off of Heavily Loaded Aircraft.

An example will be dealt with in which it will be possible:

(a) to analyse the take-off run required for present day large aircraft

(b) to establish comparative values for the analysis of assisted take-off by means of towing aircraft.

(1) *Data of the aircraft considered.*

Take-off weight	G = 60 tons
Take-off power (BMW 801)	N = 4 × 1600 H.P.
Span	b = 50 m.
Wing area	F = 352 m²
Aspect ratio $A = \dfrac{b^2}{F}$	= 7.1

Mean distance of wing from ground = 3.0 m.
Polare of aircraft (see Fig. 3).

The thickness/chord ratio of the continuous wing is 0.15, the aerofoil section is designed for high speed. The aircraft is a low-wing monoplane, with the undercarriage of the nose-wheel type. The conception, weight and dimensions closely resemble the Douglas B 19, with the execption of lower take-off weight and smaller span.

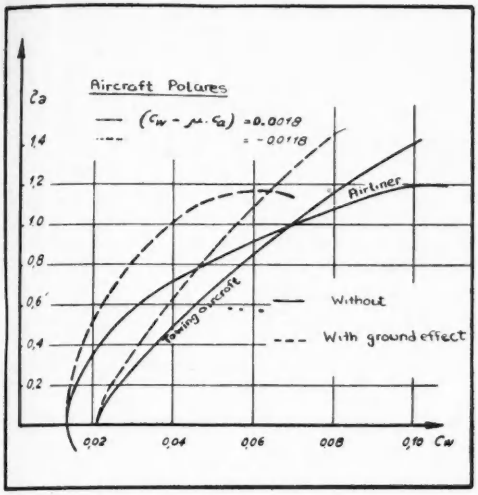

Fig. 3

The wing loading $p = \frac{G}{F} = 170$ kg./m², and is thus about 20 kg./m². higher than is customary at present. (For present day military aircraft $p = 250$ to 300 kg./m².).

The power loading of the aircraft under consideration is $m = \frac{G}{N} = 9.36$ kg./H.P., i.e., is chosen much higher than that of any modern aircraft. (Fighters, $m = 3$ to 3.5 kg./H.P., airliners and bombers $m = 5$ to 6 kg./H.P.).

(2) *Essential Factors influencing take-off.*

The angle of incidence α during the take-off run is chosen so as to make the expression $(c_w - \mu\ c_a)$ a minimum. The coefficient of ground friction μ is assumed constant and equal to 0.05.

(a) The investigation has shown that the ground effect has a very favourable influence on the aircraft polare. So, for instance, the factor $(c_w - \mu\ c_a)_{min}$ becomes negative for $\mu = 0.05$, i.e., it has not a decelarating but an accelerating effect. The vicinity of the ground reduces the induced downwash behind the wing which is due to the finite span. This is tantamount to a reduction of the induced angle of incidence, and therefore of the induced drag. This reduction of drag means an accelerating effect, i.e., the aircraft will unstick more quickly.

According to Prof. Wieselsberger the measure for the ground effect is given by

$$\frac{h}{b} = \frac{\textit{wing distance from ground}}{\textit{wing span}}$$

Dr. Daetwyler's tests confirmed this fact, and for the present example we can put

$$c_{wi\ ground} = 0.35\ c_{wi}$$

The ground effect is shown in Fig. 3, where the modified polare is shown dotted (the towed aircraft is called "Airliner"). Thus, for the take-off of such heavily loaded airliners it would be advantageous to build the wing as low as possible.

(b) The greatest effect on the length of the take-off run has the speed at unsticking. As before, we have

$$v_{ab} = \sqrt{\frac{2}{\rho} \cdot \frac{G}{F} \cdot \frac{1}{Ca_{ab}}}$$

Herein the essential factor is the wing loading $\frac{G}{F}$. In addition to the previously given aircraft data some other will have to be stated on which the following calculations are based. These are :

$c_a = 1.66$ landing flap 15 deg. deflected
$ca = 1.20\ c_{a\ max}$ without flaps
$c_a = 0.92$ at $(c_w - \mu\ c_a)_{min}$

The following are the speeds at unsticking corresponding to above lift coefficients, assuming the altitude of the airfield at 500 m. above sea level :

$c_a = 1.66$	$v_{ab} = 41.7$ m/sec.
$= 1.20$	$= 50$
$= 0.92$	$= 56$

A variation of the take-off weight G at constant lift coefficient $c_a = 1.2$ results in the following speeds :

$G = 60$ tons	$v_{ab} = 50$ m/sec.
$= 70$	$= 54$
$= 80$	$= 57.7$

Fig. 4 shows the rapid increase of the ground run with increasing v_{ab}. These curves have been calculated for constant $\frac{G}{F}$ and variable lift coefficient. Equally, c_a can be taken as constant and the wing loading variable.

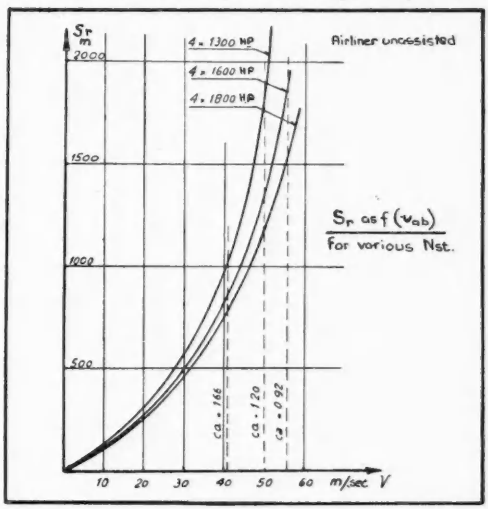

Fig. 4

(c) To a certain extent this is expressed by Fig. 5, where a variation of G has an effect on $p = \frac{G}{F}$ and $m = \frac{G}{N}$. It can be seen that the ground run increases very rapidly with increase in take-off weight.

(d) The general influence of power loading on the ground run is well expressed by the diagram (Fig. 6). It is characteristic that for low v_{ab} no worthwhile shortening of the ground run can be achieved by increase in power. Power increase for this purpose pays only at higher speeds v_{ab}. This is due to the decrease of propeller thrust with increasing speed.

By slight modification of equation (1) we can write for the acceleration :

$$\frac{dv}{dt} = g \left[\frac{S}{G} - \mu - \frac{F}{G} (c_w - \mu\ c_a)\ q \right] \quad .. \qquad (1a)$$

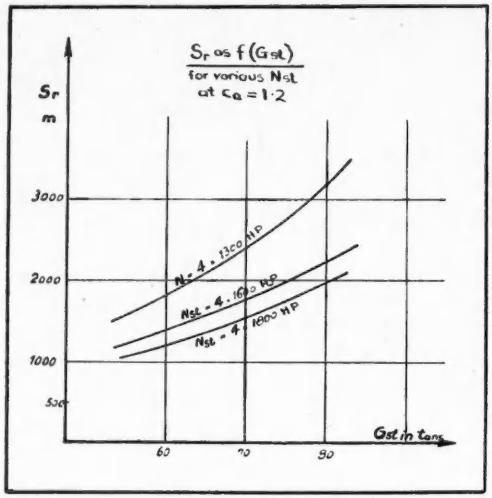

Fig. 5

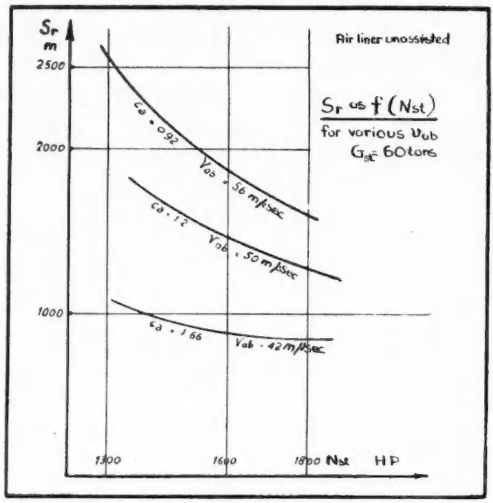

Fig. 6

Important herein is the variation of $\frac{S}{G}$, which, keeping the relation

$$S \cdot v = N_{pr} \cdot \eta_{pr} \quad .. \quad .. \quad (18)$$

in mind, can be represented as a function of the power loading.

The notation is

S = propeller thrust (kg.)
v = air speed (m./sec.)
N_{pr} = power at propeller shaft (m.kg./sec.)
η_{pr} = propeller efficiency

Thus, the thrust loading $\frac{G}{S}$ is directly proportional to the power loading $\frac{G}{N}$; the greater $\frac{G}{N}$, the smaller $\frac{S}{G}$ and the longer the ground run.

There is the same effect on the rate of climb v_{st}:

$$v_{st} = v \left(\frac{S}{G} - \frac{W}{G} \right) .. \quad .. \quad .. \quad (19)$$

and thus the angle of climb

$$\sin \varphi = \frac{S}{G} - \frac{W}{G} \quad .. \quad .. \quad .. \quad (20)$$

For our example

p = 170 kg./m²
m = 9.36 kg./H.P.(4 × 1600 H.P.)
c_a = 1.20
v_{ab} = 50 m./sec.

a ground run of s_r = 1450 m. would be required.

C. Assisted Take-off.

To begin with, the effect of a "high-powered" towing aircraft on the increase of acceleration was investigated. Subsequently, it has been found that not only was the power loading reduced, but secondary effects obtained by the strong slipstream of the propeller of the towing aircraft.

(1) *Data of the Train.*

TABLE I.

	Towing aircraft	Airliner	Train
G tons) ..	12	60	72
Nst (H.P.) ..	4 × 1600	4 × 1600	8 × 1600
b (m.) ..	28	50	
$A = \frac{b^2}{F}$ ..	11.5	7.1	
F (m²) ..	70	352	
$\frac{G}{F}$ (kg./m²)	170	170	170
$\frac{G}{N}$ (kg./H.P.)	1.875	9.36 (4 × 1600 H.P.)	5.62 (4 × 1600 H.P.)
	1.875	12.50 (4 × 1300 H.P.)	6.43 (4 × 1300 H.P.)

The ground effect on the wing of the towing aircraft has been considered, and the aircraft polare modified so that

$$\frac{c_{w1 \text{ ground}}}{c_{w1}} = 0.5$$

The coefficient of ground friction for the towing aircraft has been taken as $\mu = 0.03$.

(2) *The Take-off Equation.*

With the preliminary assumption that the speed at unsticking is equal for both aircraft, equation (1) becomes:

$$\frac{G_a + G_s}{g} \cdot \frac{dv}{dt} = S_a + S_s - q \quad [(c_w - \mu\, c_a)_s \cdot F_s + (c_w - \mu\, c_a)_a \cdot F_a] \quad - (\mu_s G_s + \mu_a G_a) \quad .. \quad (21)$$

Indices (a) and (b) refer to airliner and towing aircraft respectively.

This equation enables us to assess the improvements in take-off. With

$$S_a + S_s \geq 2 \cdot S_a$$

and $G_a + G_s = 1.2\, G_a$ (see Table I.)

the power loading is improved by 80 per cent. This already reduces the ground run of the train considerably.

(3) *Improvement by means of Increase of Take-off Thrust.*

The graphical integration of equation (21) yields the ground run S_r, whereby for variations in Airliner data those of the towing aircraft remained constant. v_{ab} corresponds always to the value given by the airliner. To obtain the effective ground run, the distance between the towing aircraft and the airliner must be added to S_r of the airliner.

(a) It is of great interest to know how far the take-off power of the airliner can be reduced without increasing the ground run of the train, as a long-distance aircraft should not take-off at maximum r.p.m. Fig. 7 shows

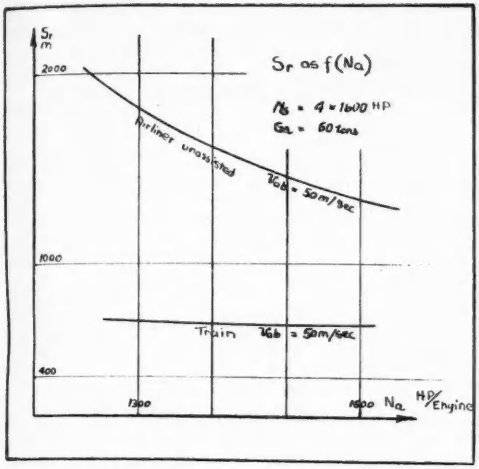

Fig. 7

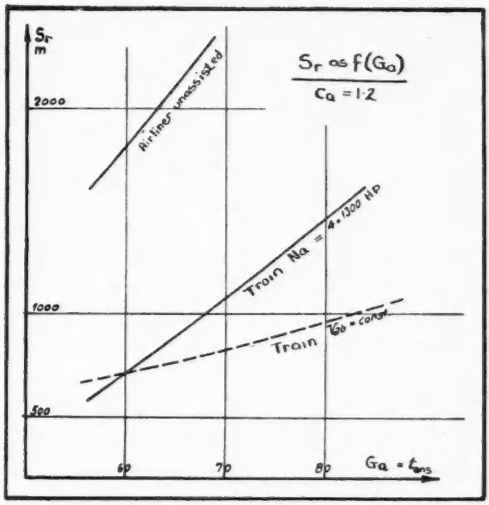

Fig. 8

that a reduction of take-off power of the airliner is practically without influence on the ground run of the train.

(b) If at reduced take-off power of the airliner its weight (G_{ast}) is increased, there is a rapid increase in the ground run. This is shown in Fig. 8. It would be possible to counteract this deterioration by increasing the lift coefficient, and the dotted curve in Fig. 8 refers to this case, when take-off in each case takes place at constant speed v_{ab}.

(c) The improved rate of climb of the train shortens also the total take-off distance as the horizontal projection S_h of the flight path from unsticking to the clearance light $h = 20$ m. decreases :

	Airliner unassisted	Train	Take-off power of airliner N_a
S_h (m)	350	126	4×1600
	500	188	4×1300

In conclusion it can be stated that in spite of a distance of say 100 m. between airliner and towing aircraft the total take-off distance of the train is about half that of the airliner alone, and thus the take-off distance is of the order of the landing run.

(4) *The Influence of the Propeller Slipstream.*

Considering the great power of the towing aircraft it is obvious that the airliner lying in its slipstream will be influenced in some way. To clear these problems model tests were made under the supervision of Prof. Dr. Ackerat (the results are omitted in this abstract, *Ed., E.D.*).

To the present problem of take-off the slipstream means to the airliner nothing more than take-off against wind, so that the effective speed

$$v_{eff} = v_z + v_{wind} \quad .. \quad .. \quad .. \quad (22)$$

where v_z = speed relative to the ground. If in our train the distance D between towing aircraft and airliner is 100 m., this would mean that the airliner would have to be accelerated to $v_z = 39$ m./sec. to reach its required $v_{ab} = 50$ m./sec.

For other coupling distances the required v_z's are as follows :

$D = 100$ m.	$v_z = 39$ m./sec.
$= 140$	$= 41.2$
$= 200$	$= 42.5$

RADIAL AND LATERAL REACTIONS ACTING UPON THE WHEELS OF A MOTOR CAR

(From E. A. TSUDAKOV'S Book, "*Theory of the Automobile*," Moscow, 1944, pp. 82-93).

(*Continued from the July issue.*)

IN the preceding instalment a method was given for the analytical determination of the total lateral reactions Y_1 and Y_2 acting upon the front and rear axles respectively of a car making a turn ; and the influence of the various factors involved was also given. Each of these lateral reactions is the sum total of the forces exerted upon the two wheels of the axle concerned. It is thus :

$$Y_1 = Y'_1 + Y''_1 \qquad Y_2 = Y'_2 + Y''_2$$

The analytical determination of the individual reactions Y' and Y'' acting upon the outside and inside wheel respectively meets, however, with considerable difficulties, since the distribution of the reactions Y_1 and Y_2 over the individual wheels depends upon a large number of factors, and in particular upon the resiliency of the tyres and of the wheels in lateral direction. If it is assumed that the resiliency of the axle and of the wheels is small as compared to that of the tyres, the distribution of the total reactions Y_1 and Y_2 over the wheels will then be directly proportional with the respective resiliencies of the tyres of outer and inner wheel. When the vehicle passes through a curve, the forces X''_1 and X''_2 acting upon the outer wheels will be greater than the forces X'_1 and X'_2 to which the inner wheels are subjected.

As the wheels are rigidly connected with the axle, the tyres will not therefore be subjected to identical conditions. However, according to test results the lateral resiliency of a tyre in practice is almost independent of the magnitude of the vertical deformation of the tyre. It may thus be assumed that with increasing values of total reaction Y the lateral reactions Y'' and Y' exerted upon inside and outside wheel respectively of an axle at first will be about equal. But if Y exceeds a certain magnitude, the tyre of the inner wheel will be slightly lifted off the ground and skidding will take place. This skidding will lead to a diminution of the lateral deformation of the tyre of the inner wheel. Con-

equently the lateral reaction Y'' exerted upon this wheel will also be diminished. At the same time the lateral reaction Y' acting upon the outer wheel will increase, because the sum total of Y' and Y'' must equal the total lateral reaction Y. If the total lateral reaction Y is increased, the reaction Y'' will be further decreased because of the skidding of the tyre of the inside wheel, and the reaction Y' will therefore increase. This variation in the lateral reactions Y'' and Y' must continue as long as both wheels do not simultaneously reach the limit of their lateral stability. If the lateral reaction actually exceeds this limit, both wheels of the axle will begin to skid.

If the wheels of the axle are free of circumferential forces, the lateral reactions prevailing will be given by $Y'' = \varphi \,.\, X''$ and $Y' = \varphi \,.\, X'$. But as the sum total of the lateral reactions must always be equal to the total reaction Y which acts upon the axle, it must also be $Y = Y' + Y'' = \varphi\,(X' + X'') = \varphi \,.\, X$, where X is the total of the radial reactions acting upon the axle concerned. This interrelationship constitutes the criterion for the conditions under which skidding of the wheels will occur. However, if inertial or braking forces are transmitted by the wheels to the axle, the aforementioned equation will cease to apply, and it will then be necessary to ascertain the lateral reactions acting upon each wheel of the axle.

In order to verify the assumptions made above with regard to the variation of the two lateral reactions Y' and Y'' with increasing magnitude of the total lateral reaction Y, a special test was carried out, using the set-up outlined in Fig. 13. Here the cable (6) serves to apply the lateral force, with the axis of the cable passing through the centre of gravity of the vehicle. The magnitude of the lateral force is adjusted by means of the manually operated screw spindle. (8) The force applied is indicated by the measuring device (7). The left hand side rear wheel of the automobile is placed upon a base plate (4) resting on the platform of the balance (5). This base plate is supported on steel balls in order to make it freely movable in all directions.

The lateral force Y'_2 acting upon the wheel is represented by the tension of the cable (3) attached at one end to the base plate (4). The tension of the cable is controlled by the handwheel of the spindle carried in the pedestal (1). The amount of tension applied is indicated by the dynamometer (2). In this way the total lateral force applied at the centre of gravity of the car is indicated by the dynamometer (7). The vertical (radial) reaction X'_2 acting upon the rear wheel is measured by means of the balance (5); while the dynamometer (2) serves to measure the lateral reaction Y''_2.

In order to ascertain the influence of the degree of inflation of the tyres upon the variations in radial and lateral reactions exerted upon the vehicle, test runs were made with different tyre pressures and also with tyres of different profiles. Tyres of 28 × 4.74 in. were inflated to 1.8 and 2.2 atm. pressure, while tyres of 29 × 5.5 in. were inflated to 2.0 atm. pressure. Moreover, in order to ascertain to what extent the lateral and radial reactions are influenced by the resiliency of the springs, test runs were also made with and without the use of shock absorbers. As will be seen from the test data given below, changes in the tyre pressures (within the limits indicated) or in the tyre dimensions, or the application of shock absorbers, do not produce any significant variations in the distribution of the lateral and radial reaction forces acting upon the wheels.

The test data obtained are charted in Figs. 14-17, which show the variations in the reaction forces Y'_2 and Y''_2 as function of the total lateral force N applied to the vehicle by means of cable (6) (Fig. 13). According to

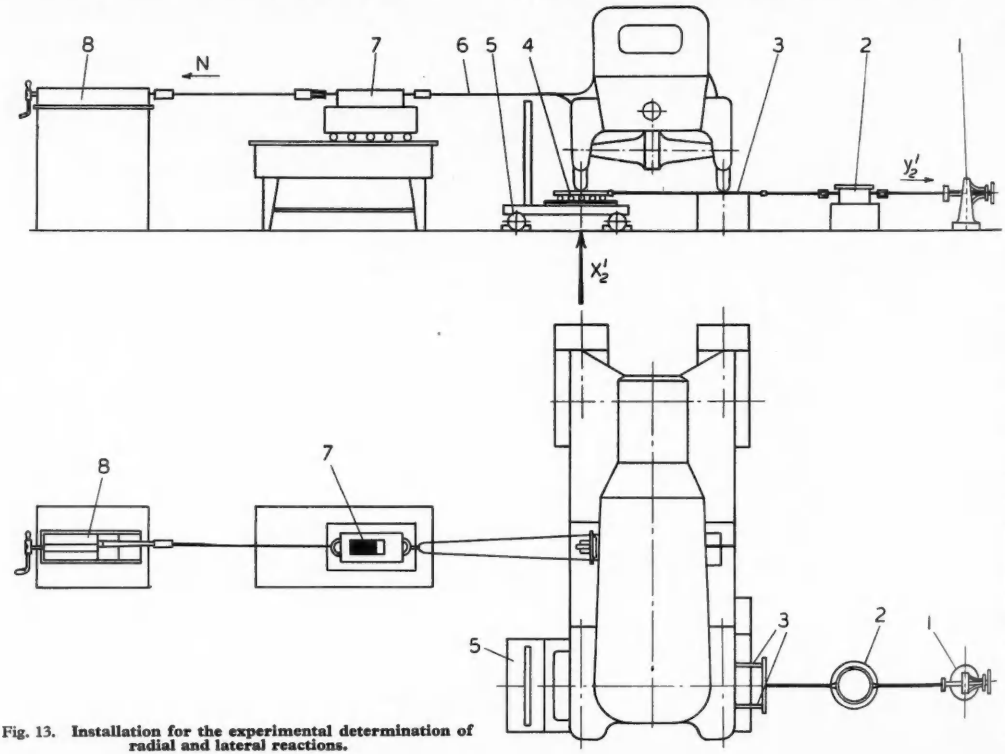

Fig. 13. **Installation for the experimental determination of radial and lateral reactions.**

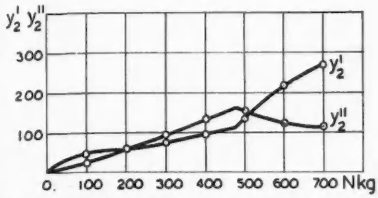

Fig. 14. **Relationship between lateral force N and lateral reactions $Y'2$ and $Y''2$. Tyres 28×4.75 in. at 1.8 atm. pressure. Shock absorbers in place.**

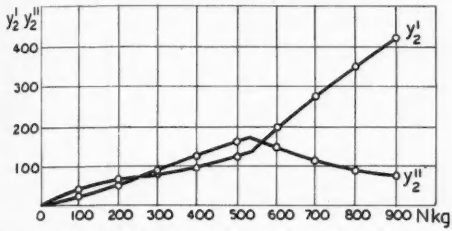

Fig. 16. **Relationship between lateral force N and lateral reactions $Y'2$ and $Y''2$. Tyres 29×5.5 in. at 2.0 atm. pressure. Shock absorbers in place.**

these charts the respective values of the lateral reactions Y'_2 and Y''_2 differ but little up to the point where the inside wheel begins to slip. With a further increase in the force N, and with it in the total reaction Y, the reaction Y''_2 begins to rise steeply. It will be appreciated that this decrease in the reaction Y''_2 is the result of the decrease in the radial reaction X''_2. Slipping of the inside wheel commences when N is increased to 475 kg. if 28 × 4.75 in. tyres are fitted and when N is increased to 525 kg. if 29 × 5.5 in. tyres are used. At the instant of incipient slipping the lateral reaction Y''_2 approximates to 150 kg. By also recording the magnitude of the radial reactions X'_2 and X''_2 which act upon the outer and inner wheels of the axle, the magnitude of the coefficient φ at the instant of incipient slippage can be determined. The results of tests conducted to de-

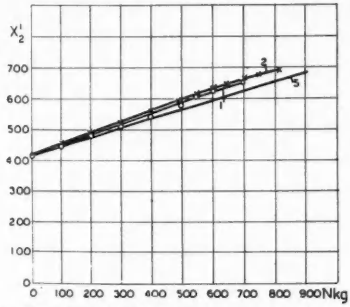

Fig. 18. **Experimental determination of $X'2$ *versus* N for inside wheel of rear axle.**

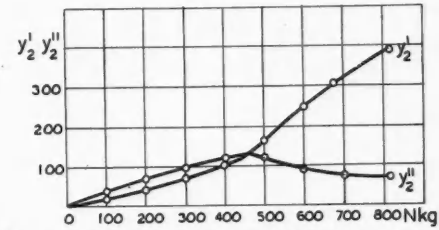

Fig. 15. **Relationship between lateral force N and lateral reactions $Y'2$ and $Y''2$. Tyres 28×4.75 in. at 2.2 atm. pressure Shock absorbers in place.**

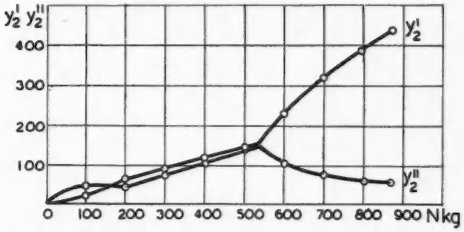

Fig. 17. **Relationship between lateral force N and lateral reactions $Y'2$ and $Y''2$. Tyres 29×5.5 in. at 2.0 atm. pressure. Shock absorbers removed.**

termine the radial reactions will be referred to below. According to these results the radial reaction X''_2 prevailing at the instant of incipient slipping of the inside wheel amounts to 260 kg. with the coefficient φ attaining a value of 0.6. Experimentally obtained values for the radial reaction X'_2 as function of the lateral force N are shown in Figs. 18 and 19. These values were used in charting Figs. 14-17. The loading of the rear axle amounted to 840 kg. The coefficient φ is therefore given by the expression $\varphi = \dfrac{Y''_2}{X''_2} = \dfrac{Y''_2}{840 - X'_2}$.

The computed values of φ are charted in Fig. 20. Referring to this graph it will be seen that the coefficient

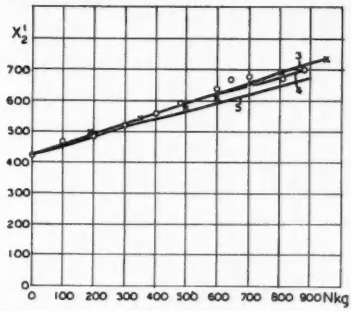

Fig. 19. **Experimental determination of $X'2$ *versus* N for inside wheel of rear axle.**

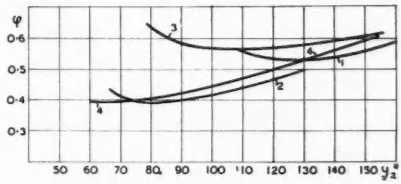

Fig. 20. **Relationship between coefficient φ and lateral reaction $Y2$.**

φ varies within rather wide limits. This is explained by the fact that during the test the speed of slipping of the inside wheel could not be maintained constant.

In the case of the rear axle the distribution of the total lateral reaction depends not only upon the radial reactions X' and X'', but also upon the traction forces P'_p and P''_p exerted upon the wheels of the axle. In view of the fact that the respective values of P'_p and P''_p depend upon the design of the differential, it follows that the radial reactions X'_2 and X''_2 also depend upon the design of the drive. But, in any event, the reaction X''_2 will of course be smaller than X'_2.

It may at first be assumed that the motion of the axles takes place without the exertion of a propulsion force (i.e., $P'_p = P''_p = 0$), and that the lateral force Y_2 is so small that the inside wheel has not yet begun to skid. In this case the reaction forces Y'_2 and Y''_2 may be identical, as was explained above. It may further be assumed that a gradually increasing total propulsive force P_p is transmitted through the axle which imparts the propulsive forces P'_p and P''_p to the wheels. For a certain magnitude of the propulsive force P_p the resultant reaction R''_2 will attain the same magnitude as the force $\varphi \cdot X''_2$ and the inside wheel will then slip on the ground. This will result in a decrease in the lateral reaction Y''_2 and consequently in an increase in the lateral reaction Y'_2. This phenomenon of a diminishing lateral reaction Y''_2 and simultaneously increasing reaction Y'_2 will go on until one of the two reactions disappears altogether. In this way either the lateral reaction Y''_2 will decrease to zero, or both wheels, and therefore also their axle, will slip sideways.

DETERMINATION OF RADIAL REACTIONS ACTING UPON THE WHEELS OF FRONT AND REAR AXLE.

The radial reactions may be defined as the forces which act upon the wheels of the vehicle in perpendicular direction upon the peripheral surfaces of the wheels, that is to say, in radial direction. A diagram of the forces acting upon a vehicle making a turn is given in Fig. 21, where G is the weight of the vehicle acting at the height h_g above the ground level, P_w is the force of air resistance applied at the height h_w above the ground level, X'_1 is the radial reaction acting upon the outside wheel of the front axle, X''_1 is the radial reaction acting upon the inside wheel of the front axle, X'_2 is the radial reaction acting upon the outside wheel of the rear axle, X''_2 is that acting upon the inside wheel of the rear axle, q'_1, q''_1, q'_2, q''_2 are the respective forces of rolling friction acting upon the wheels, and Mc'_1, Mc''_1, Mc'_2, Mc''_2 are the respective moments of rolling resistance acting upon the wheels of the vehicle.

Referring to Fig. 21 it will be seen that the resisting forces q'_1 and q''_1 and the moments Mc'_1 and Mc''_1 will be a function of the angle α enclosed by the steering wheel, i.e., the front axle, and the longitudinal axis AB of the vehicle. But if the vehicle travels along a road offering little rolling resistance, the forces q'_1 and q''_1 as well as the moments Mc'_1 and Mc''_1 will be very small. For practical purposes it may therefore be assumed that these forces and moments act in the direction of the length axis of the vehicle. No serious error will therefore be incurred in using the equation

$$(X'_1 + X''_1)\, L + Mc'_1 + Mc''_1 + Mc'_2 + Mc''_2 + T \cdot h_g + P_w \cdot h_w - G \cdot b = 0 \quad .. \quad (26)$$

where the sum total of the moments is given by

$$Mc'_1 + Mc''_1 + Mc'_2 + Mc''_2 = (q'_1 + q''_1 + q'_2 + q''_2)\, r = f\,(X'_1 + X''_1 + X'_2 + X''_2)\, r \quad .. \quad (27)$$

In this equation f denotes the coefficient of rolling resistance, and r is the radius of the wheels. But it is also $X'_1 + X''_1 + X'_2 + X''_2 = G$, and by substitution in equation (27) it obtains

$$Mc'_1 + Mc''_1 + Mc'_2 + Mc''_2 = f \cdot G \cdot r \quad .. \quad (28)$$

The equilibrium condition of all the forces projected upon the longitudinal axis of the vehicle is given by

$$P_p' + P_p'' = T + q'_1 + q''_1 + q'_2 + q''_2 + P_w + Y_1 \sin\alpha$$

or

$$\gamma_p \cdot G = T + P_w + f \cdot G + Y_1 \sin\alpha \quad .. \quad (29)$$

By combining the equations (26) and (29) and making $h_g = h_w$ (which is quite permissible for practical purposes), it obtains

$$X'_1 + X''_1)\, L = G \cdot b - \gamma_p \cdot h_g \cdot G + f \cdot G\,(h_g - r) + Y_1 \cdot h_g \cdot \sin\alpha \quad .. \quad .. \quad (30)$$

which applies to the front axle. The corresponding expression applying to the rear axle will then be

$$(X'_2 + X''_2)\, L = G \cdot a + \gamma_p \cdot h_g \cdot G - f \cdot G\,(h_g - r) - Y_1 h_g \cdot \sin\alpha \quad .. \quad .. \quad (31)$$

If the vehicle travels on a smooth road, the coefficient of rolling resistance will be very small and approximate to $f = 0.015$. Furthermore, if the car travels at high speed, the angle α will also be very small. By neglecting the third and fourth members of the right hand sides of equations (30) and (31), the radial reactions X_1 and X_2 will then be given by

$$X_1 \cdot L = (X'_1 + X''_1) \cdot L = G \cdot b - \gamma_p \cdot h_g \cdot G \quad .. \quad (32)$$

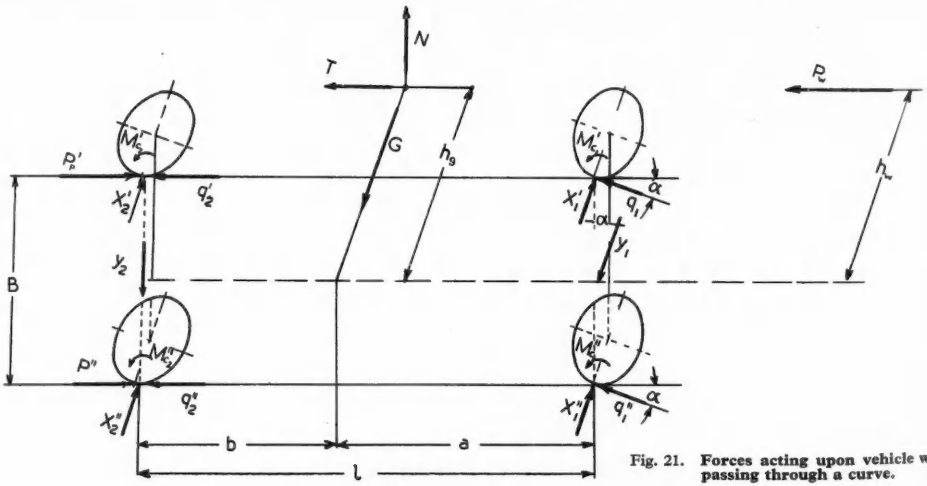

Fig. 21. **Forces acting upon vehicle when passing through a curve.**

$$X_2 \cdot L = (X'_2 + X''_2) \cdot L = G \cdot a + \gamma_p \cdot h_g \cdot G \quad .. \quad (33)$$

By introducing the coefficients of weight distribution m_1 and m_2, it becomes

$$X_1 = m_1 \cdot G_1 \; ; \; X_2 = m_2 \cdot G_2 \quad .. \quad .. \quad (34)$$

where G_1 is the weight of the vehicle resting upon the front axle and G_2 is that supported by the rear axle. The coefficients m_1 and m_2 can then be found with sufficient accuracy from the equations

$$m_1 = 1 - \gamma_p \frac{h_g}{b} \quad .. \quad .. \quad .. \quad (35)$$

$$m_2 = 1 + \gamma_p \frac{h_g}{a} \quad .. \quad .. \quad .. \quad (36)$$

The total radial reactions X_1 and X_2 as well as the individual reactions X'_1 ; X''_1 ; X'_2 and X''_2 are functions not only of the lateral force N and of the disposition of the centre of gravity of the vehicle, but their magnitude also depends upon the rigidity of the body, frame, springs, and tyres of the vehicle, and also upon the distance between the springs of front and rear axle.

Referring to Fig. 22, the lateral force N—determined by equation (11)—applies at the centre of gravity of the vehicle in a plane parallel with the ground level, as indicated in Fig. 21. The forces acting upon front and rear axle of the car, and the deformations of the springs are shown in the diagrams (Figs. 23 and 24). The distance between the springs of the front axle is given as l_1 and that of the rear axle as l_2. The force N exerts a moment $N \cdot h_1$ upon the frame, which is composed of a moment M_1 acting upon the front part of the frame and taken up by the front springs λ_1 and of a moment M_2 acting upon the rear part of the frame and taken up by the rear springs λ_2 (Figs. 23 and 24). The magnitude of the radial reactions X acting upon the wheels obviously depends upon the relative magnitude of the moments M_1 and M_2 taken up by the front and rear springs respectively and by the respective axles. The relative magnitude of the moments M_1 and M_2 will depend upon the resiliency of the frame, the springs, and of the tyres ; and the resiliency of these parts in turn will determine the magnitude of the radial reactions X acting upon the wheels of the car.

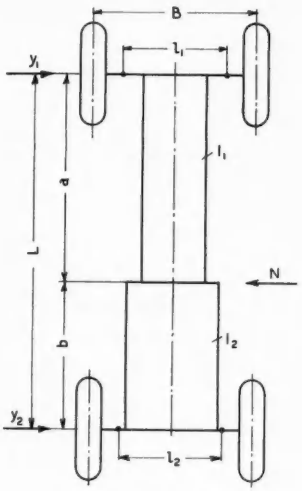

Fig. 22. **Forces acting upon vehicle when passing through a curve.**

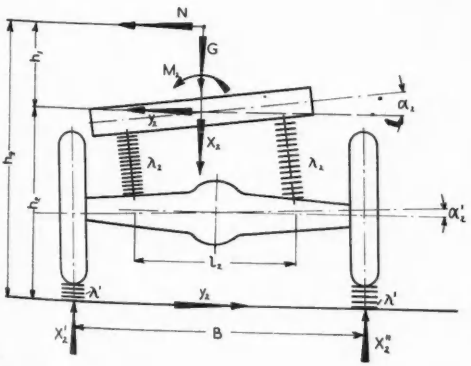

Fig. 23. **Deformation of springs and tyres of car passing through a curve.** (Rear axle).

By introducing the moments of inertia I_1 and I_2 (Fig. 22) it will be possible to establish the relationship between the moments M_1 and M_2, expressed as a function of the resiliency of the springs and of the tyres, and of the distances l_1 and l_2 between the springs. It may further denote :

λ_1 = coefficient of resiliency of the springs of front axle.
λ_2 = coefficient of resiliency of the springs of rear axle.
λ' = coefficient of resiliency of the tyres
α_0 = angle of inclination of the frame with the horizontal owing to the application of the force N and measured in the plane in which the force N applies.
α_1 = angle of inclination of the frame with the horizontal, measured in the vertical plane passing through the front axle of the vehicle
α_2 = angle of inclination of the front axle of the car relative to the horizontal
α'_2 = angle of inclination of the rear axle relative to the horizontal.

The elastic deformation of the front part of the frame, subjected to the moment M_1 is seen to be $(\alpha_0 - \alpha_1)$, and the moment M_1 therefore is

$$M_1 = (\alpha_0 - \alpha_1) \frac{I_1 G}{a} \quad .. \quad .. \quad .. \quad (37)$$

where G is the modulus of elasticity in shear. The angle of distortion of the front axle relative to the frame, which is due to the elastic deformation of the springs, is $(\alpha_1 - \alpha'_1)$, and it therefore becomes

$$M_1 = \lambda_1 \cdot (\alpha_1 - \alpha'_1) \frac{l_1^2}{2} \quad .. \quad .. \quad (38)$$

Furthermore, the moment M_1 can also be expressed

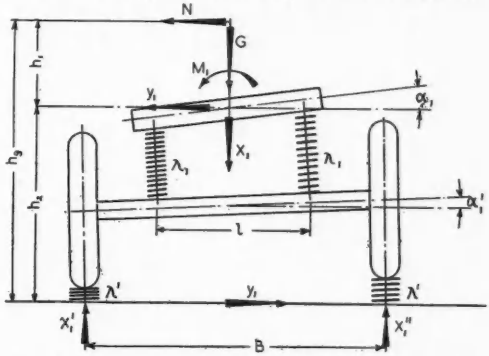

Fig. 24. **Deformation of springs and tyres of car passing through a curve.** (Front axle).

as function of the angle α'_1, the wheel gauge B, and the coefficient of tyre resiliency λ', to wit :—

$$M_1 = \lambda' \cdot \alpha'_1 \cdot \frac{B^2}{2} \quad \ldots \quad \ldots \quad \ldots \quad (39)$$

Combining equations (37) (38) and (39), we obtain

$$M_1 = \frac{\alpha_o}{\frac{a}{l_1 \cdot G} + 2\left(\frac{1}{\lambda_1 l_1^2} + \frac{1}{\lambda' B^2}\right)} \quad \ldots \quad (40)$$

Similarly, the moment M_2 can be expressed by

$$M_2 = (\alpha_o - \alpha_2) \frac{I_2 \cdot G}{b}$$

and $$M_2 = \lambda_2 (\alpha_2 - \alpha'_2) \frac{l_2^2}{2}$$

and $$M_2 = \lambda' \cdot \alpha'_2 \cdot \frac{B^2}{2}$$

and combining

$$M_2 = \frac{\alpha_0}{\frac{b}{I_2 \cdot G} + 2\left(\frac{1}{\lambda_2 l_2^2} + \frac{1}{\lambda' B^2}\right)} \quad \ldots \quad (41)$$

It follows that the relationship between M_1 and M_2 is expressed by

$$M_1 \left[\frac{a}{I_1 \cdot G} + 2\left(\frac{1}{\lambda_1 l_1^2} + \frac{1}{\lambda \cdot B^2}\right)\right] = M_2 \left[\frac{b}{I_2 \cdot G} + 2\left(\frac{1}{\lambda_2 l_2^2} + \frac{1}{\lambda^1 B^2}\right)\right] \quad (42)$$

The sum total of M_1 and M_2 is defined as

$$M_1 + M_2 = (Y_1 + Y_2) h_1 = N \cdot h_1$$

where h_1 is the elevation of the centre of gravity relative to the frame of the vehicle (Fig. 24). It will therefore be

$$M_1 = N \cdot h_1 \frac{\frac{b}{I_2 G} + 2\left(\frac{1}{\lambda_2 l_2^2} + \frac{1}{\lambda' B^2}\right)}{\frac{a}{I_1 G} + 2\left(\frac{1}{\lambda_1 l_1^2} + \frac{1}{\lambda' B^2}\right) + \frac{b}{I_2 G} + \left(\frac{1}{\lambda_2 l_2^2} + \frac{1}{\lambda' B_2}\right)} \quad (43)$$

and

$$M_2 = N \cdot h_1 \frac{\frac{a}{I_1 G} + 2\left(\frac{1}{\lambda_1 l_1^2} + \frac{1}{\lambda^1 B^2}\right)}{\frac{a}{I_1 G} + 2\left(\frac{1}{\lambda_1 l_1^2} + \frac{1}{\lambda^1 B^2}\right) + \frac{b}{l_2 G} + 2\left(\frac{1}{\lambda_2 l_2^2} + \frac{1}{\lambda^1 B^2}\right)} \quad (44)$$

The flexibility of the frame and the body of the vehicle usually is very small as compared to that of the springs and of the tyres. No serious error will therefore be introduced by neglecting the terms $\frac{b}{I_2 G}$ and $\frac{a}{I_1 G}$. The equations for M_1 and M_2 will then take the form :

$$M_1 = N \cdot h_1 \frac{1}{1 + \frac{\lambda_2 l_2^2 (\lambda^1 B^2 + \lambda_1 l_1^2)}{\lambda_1 l_1^2 (\lambda^1 B^2 + \lambda_2 l_2^2)}} \quad \ldots \quad (43a)$$

$$M_2 = N \cdot h_1 \frac{1}{1 + \frac{\lambda_1 l_1^2 (\lambda^1 B^2 + \lambda_2 l_2^2)}{\lambda_2 l_2^2 (\lambda^1 B^2 + \lambda_1 l_1^2)}} \quad \ldots \quad (44a)$$

If it is further assumed that the resiliency of the springs is considerably less than that of the tyres, so that

$$\lambda^1 B^2 + \lambda_1 l_1^2 = \lambda^1 B^2 + \lambda_2 l_2^2$$

the moments M_1 and M_2 can then be expressed by

$$M_1 = N \cdot h_1 \frac{1}{1 + \frac{\lambda_2 l_2^2}{\lambda_1 l_1^2}} \quad \ldots \quad \ldots \quad (43b)$$

$$M_2 = N \cdot h_1 \frac{1}{1 + \frac{\lambda_1 l_1^2}{\lambda_2 l_2^2}} \quad \ldots \quad \ldots \quad (44b)$$

Having thus determined the moments M_1 and M_2 and also the reactions Y_1 and Y_2 which act upon front and rear part respectively of the frame, the resultant counteracting radial reactions ΔX_1 and ΔX_2 can then be found from

$$\Delta X_1 = \frac{M_1 + Y_1 h_2}{B} \quad \ldots \quad \ldots \quad \ldots \quad (45)$$

$$\Delta X_2 = \frac{M_2 + Y_2 h_2}{B} \quad \ldots \quad \ldots \quad \ldots \quad (46)$$

These expressions determine the amounts by which the radial reactions acting upon the outside wheels of the vehicle are increased, and by which the radial reactions exerted upon the inside wheels are decreased. But these equations give only a very approximate solution of the problem and can furnish no more than a very sketchy illustration of the influence of the various factors involved.

A precise analytical determination of the moments M_1 and M_2 and with it an exact analytical determination of the radial reactions acting upou the wheels when the car passes through a curve, is hardly possible. This is due to the fact that the flexibility of the frame and of the body is not uniform over the length of the vehicle.

THE APPLICATION OF THE COMBUSTION TURBINE TO THE PROPULSION OF SHIPS.

By R. SCHMID. (From *Brown Boveri Review*, Vol. 31, No. 10, October, 1944, pp. 350-352).

THE following comments should enable the specialist to form an independent opinion on the economical value of combustion turbines for the propulsion of ships :

(*a*) The design is simple and all parts are easily accessible.

(*b*) Attendance and maintenance do not present any problems for the operating staff.

(*c*) The rotating parts run smoothly and without vibration and are subject to practically no wear. The expenses for spare parts are small.

(*d*) Depending upon the degree of economy required, it is possible to build the combustion turbine plant for a fuel consumption of 350 to 220 grams/S.H.P.h., corresponding to an efficiency range of about 18 to 29 per cent.

(*e*) All kinds of fuel oil which can be burnt in ordinary boilers can be used for the combustion turbine.

(*f*) The weight is lower, and the space required is smaller, than that of any other propelling machinery.

(*g*) The combustion turbine has proved itself for mobile plants under much more difficult conditions than those met in propelling ships.

Since the gas turbine is superior to the best steam plants in regard to both efficiency and weight, there remains only the Diesel engine for comparison. In calculating the economic value of the Diesel engine the costs of lubricating oil must be taken into account as these may amount to 5 to 20 per cent of the cost of the fuel. In the case of gas turbines the consumption of lubricating oil is negligible. The nomogram (Fig. 1) enables the relationship between the thermal efficiency and the costs of fuel and lubrication oil for the Diesel engine and the combustion turbine to be easily investigated. With the usual prices for fuel and lubricating oil, the parity price for fuel oil lies around 60 to 70 per cent of the price of Diesel oil. Basing on the pre-war fuel prices, the combustion turbine could accordingly compete with the Diesel engine on by far the greater number of maritime routes. Though no predictions are possible in regard to the post-war fuel prices, already a small difference between the prices of Diesel oil and fuel will be sufficient to assure an economically advantageous position of the combustion turbine for the propulsion of ships.

An important point of view when planning a ship is the question of the weight of the machinery and of the fuel load. Since the combustion turbine is considerably lighter than a Diesel engine, but consumes a little more fuel, it follows that for voyages less than a certain distance, the combustion turbine is more advantageous, but on the other hand the lower consumption of the Diesel engine makes the latter more advantageous for very long voyages. For a certain duration of the voyage the sum of fuel and machinery weights for a gas turbine plant will be the same as for Diesel engine machinery. For average values this " equivalent duration of voyage " is :

$$\frac{(65 - 25)\ \text{kg./S.H.P.}}{(0.235 - 0.165)\ \text{kg./S.H.P.h.} \times 24} = \text{about 24 days.}$$

Basing on a speed of 14 knots and a single fuel loading, parity of weights is, therefore, obtained for a return trip of about 8,000 nautical miles.

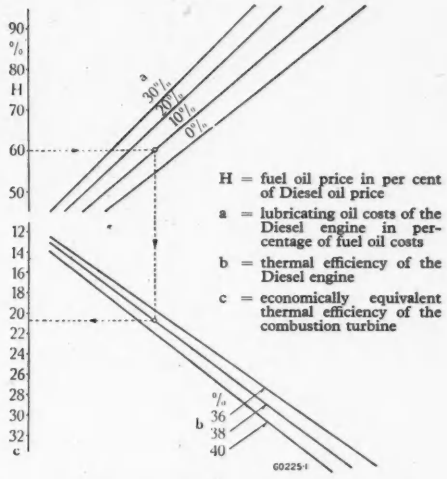

Fig. 1 — Nomogram for comparing the economy of the Diesel engine with the combustion turbine.

As for the transmission of power to the propeller shaft it has been found that the most suitable arrangement is with a variable pitch propeller. An astern turbine is then not necessary and the combustion turbine can be operated throughout the load range and during manoeuvering at its most suitable speed. According to the latest experience variable pitch propellers can be built satisfactorily for large as well as small powers.

DEVICE FOR MEASURING THE ANGLE OF TWIST OF SHAFTS REVOLVING AT HIGH SPEEDS

By R. BAUDER. (From *Elektrotechnik und Maschinenbau*, Vol. 61, Nos. 27/28, July 1943, pp. 311-314.

IN mechanical power transmissions it is frequently desired to measure the power N transmitted from one shaft to another, or failing this, to determine it indirectly by measuring the torque M_d, the angular velocity ω_w, and the speed n :

$$N = \omega_w \,.\, M_d\ ;\ N = \frac{M_d \,.\, n}{71650}\ \text{HP} = \frac{M_d \,.\, n}{97360}\ \text{kW} \quad (1)$$

n .. r.p.m., M_d .. kg. cm., H.P. .. metric horse power While, for speeds up to 3000 r.p.m. there are available a great number of instruments and methods which enable satisfactory measurement of N, M_d and n, it becomes increasingly difficult to determine these three entities at high speeds (up to 30000 r.p.m.) The explanation of this fact is given by the increase of the centrifugal force with the square of the speed. Not only strength but absolute symmetry of the measuring parts is required, and these must be limited in radial direction. It is well to recall that, e.g., the mass of one gramm weight at a radius of 5 cm. at $n = 30000$ r.p.m., produces a centrifugal force of 50 k.g.

Existing torque meters are based on the principle of torsion within the elastic range a gauge length (say a clutch shaft) being applied for the transmission of the torque to be measured.

The angle of twist (α deg.) of the cylindrical gauge length is given as :

$$\alpha = \frac{360}{2\pi} \cdot \frac{M_d \,.\, L}{G \,.\, I_p} = 585\ \frac{M_d \,.\, L}{G\, D^4} \quad .. \quad (2)$$

α = angle of twist (deg.)
I_p = polar moment of inertia (cm⁴.)
M_d = torque (kg. cm.)
G = shear modulus (kg./cm.².)
L = gauge length (cm.)
D = shaft diameter (cm.)

In the elastic range G = const., and after choosing L and D

$$\alpha = \text{const.} \times M_d \,.. \quad .. \quad .. \quad (3)$$

In the following a new method of torque measurement will be described which satisfies the requirements due to high speed. These requirements are :

1. A minimum of alterations to be made in the design of the rotating parts of the component parts required for measuring.
2. Minimum dimensions of these members in radial direction.
3. Minimum pointer width and great scale lengths.

Fig. 1 shows how the rays from the light sources Q_1 and Q_2 after passing slots B_1 and B_2 impinge on the mirrors S_1 and S_2 which are mounted on shaft W. When W rotates the rays are reflected simultaneously—or in the presence of twist, with a time lag—through slots B_3 and B_4 into the photocells P_1 and P_2, where they produce photo electric currents. These currents are led to the cylindrical deflection-system C of a cathode ray oscillograph PO. Hereby radial deflections are added to the basic motion of the cathode ray, so that on the screen a bright circle appears with humps Z_1 and Z_2. The distance of the humps Z_1 Z_2 is a measure of the

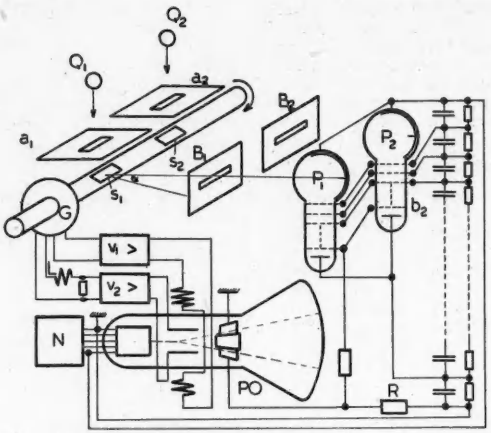

Fig. 1. Schematic representation of the new measuring method.
Q light sources, *B* slots, *S* mirror, *W* shaft, α angle of twist, *G* double generator, *P* photo-cells with secondary election amplifiers, C_s accumulator condensers, *T* tension divider, *V* amplifier, *L* inductance, *R* ohm's resistances, *PO* polar coordinate oscillograph, *F* deflection plates, *E* deflection coils, *C* cylinder condenser for radial deflection, *N* mains apparatus.

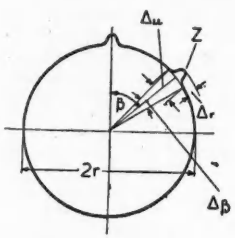

Fig. 2. Image with humps.
Z humps, Δr height of hump, Δn hump root, $\Delta\beta$ limiting angle of hump root, β screen angle, *r* radius of image.

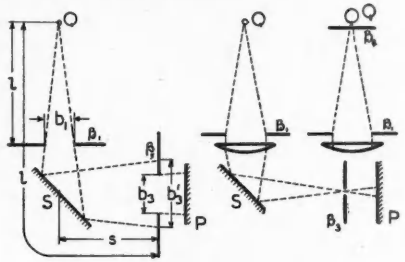

Fig. 3. Optical arrangement.
Q light sources, *B* slots, *S* mirror, *P* photo-cells, *b* slot width, *b'* width of light beam, *l* distances of light source from slots, *s* distance of mirror centre from slot β_3.

angle of twist α for the gauge length $S_1 S_2$ of shaft *W*. For an equal angular speed of shaft and circular motion of the light spot, on angle β (screen angle) appears on the screen which corresponds with the angle of twist ($\beta = \alpha$). To obtain a stationary image, the condition is $\omega_s = p\,\omega_w$, where ω_b = anguiar speed of light spot, ω_w = angular speed of shaft, and p an even number. Then,

$$\beta = p \,.\, \alpha \quad .. \quad .. \quad .. \quad (4)$$

In the present method the radial deflection of the cathode ray represents the pointer tip (Fig. 2.) Suitable optical arrangements are shown diagrammatically in Fig. 3. If the angle through which mirror *S* must turn from the beginning to the end of the cell exposure is denoted by $\Delta\alpha$, the limiting angle of the hump root is $\Delta\beta = p\ \Delta\ \alpha$ (see Fig. 2). For the optimum case of slot width equal to width of light beam, $b_3 = b_3'$, and with $\Delta\beta$ in degrees we obtain

$$b_3 = \frac{\pi \,.\, \Delta\beta \,.\, s}{180 \,.\, p} \quad .. \quad .. \quad .. \quad (5)$$

where *s* is the distance from mirror centre to slot B_3.

Putting approximately $s \cong l_3 - l_1$ (l_1, l_3 = distances of slots B_1, B_3 from light source Q_1), we have

$$l_1 = \frac{1}{\dfrac{\pi \,.\, \Delta\beta}{180 \,.\, p \,.\, b_1} - \dfrac{1}{s}}$$

Example: $r = 57$ mm.; $\Delta u = 1$ mm.; i.e., $\Delta\beta = 1$ deg.; $b_1 = 0.3$ mm.; $p = 5$; $s = 140$ mm.; $l_1 = 225$.

If Φ is the amount of lignt in Lumen, emanating from the light source *Q*, we have in the optimum case $b_3 = b_3'$

$$\Delta\Phi_{max} = \frac{\Phi \,.\, a_1 \,.\, b_1}{4\,\pi\, l_1^2}\, Lm \quad .. \quad .. \quad (7)$$

the amount of light reaching the photo-cell (a_1 = length of slot B_1). For incandescent bulbs we can assume $10Lm/W$, and with a 25 watt bulb, and $a_1 = 15$ mm., $\Delta\Phi_{max} = 2.5 \times 10^{-3}$, taking again the aforementioned example. The photo-layer of *P* (Fig. 1) receives but 1 *mLm*. Therefore rhodium plated mirrors are recommended.

The time Δt required for one hump in the image is

$$\Delta t = \frac{30 \,.\, b_1}{\pi \,.\, n \,.\, s} \quad .. \quad .. \quad .. \quad .. \quad (8)$$

For a speed $n = 30000$ r.p.m., and the previous example $\Delta t = 0.7\ \mu$ sec.

The "Fernseh-GmbH" built an apparatus based on the aforementioned principles which satisfied all expectations as it enabled at 30000 r.p.m. to take readings to $\pm$ 0.2 deg. accuracy.

PROPERTIES OF HIGH TEMPERATURE ALLOY STEELS

By C. I. WOLFSON and M. P. MJAKOV. (From *Stal*, No. 3-4, 1943, pp. 42-47).

STEELS for apparatus and high pressure lines operating at high temperature must possess the following properties :—

(1) At room temperature bolting material must possess a high yield point and satisfactory ductility.

(2) Its toughness must be sufficiently high at elevated temperature.

(3) Its initial deformation must be a minimum, while its creep must be as small as possible under sufficiently high tensile stress.

(4) Steel used for bolting material must be free from grain coarsening.

(5) Its hot working properties must not deteriorate with increasing temperature.

One of the special steels formerly most frequently used as bolting material was the Cr-Ni steel with 0.25-0.45 C, 0.5-1.5 Ni, 0.5-0.75 Cr. However, when used as bolting material for the comparatively low temperature of 400 deg. C, this steel did not come fully up to expectations, and other steels are now being employed, as, for instance, a molybdenum steel with 0.4-0.5 C, 1.0-1.5 Cr, 0.4-0.6 Mo, or a molybdenum steel with 0.28-0.35 C, 2.3-2.8 Ni, 0.5-0.7 Cr, 0.6-0.8 Mo.

In the present investigations into the suitability of alloy steels as bolting material, both structural steels and tool steels have been examined. In appreciation of the fact that the materials considered are to operate at high temperature, their heat treatment has been so devised that the tempering temperature is not less than 100 deg. C in excess of the actual operating temperature. This precaution ensures adequate stability under operating conditions. A tabulation of the steels investigated and of their composition, their heat treatment, and also of their mechanical properties is given in the subjoined Table 1.

In Fig. 1 is shown the short-time strength of these materials, and it is seen that steel No. 5 is the least strong of the materials tested. The chrome-silicon steel, Z4XC, and the chrome-silicon-manganese steel, ZI 179, retain high short-time strength up to 450 deg. C. Their short-time strength, however, decreases quickly if this temperature is exceeded, and at 600 deg. C the short-time strength of steel ZI 179 is only approximately that registered with the plain carbon steel St. 5. At 300-450 deg. C the Cr-Mo steel ZOXMA and the Cr-Mo-Al material Z5XM10A show lower short-time tensile strength than the material Z4XC, ZI179, Z10, etc., but they have relatively higher short-time tensile

TABLE I.

Type of Steel	No.	Composition, %									Heat Treatment	U.T.S. kg./ sq.mm.	Y.P. kg./ sq.mm.	0.01 % Y.S. kg./sq. mm.	Elongation, %	Reduction of Area, %	Brinell Hardness	Impact Strength Charpy, K.G.M. /sq.cm.
		C	Mn	Si	Ni	Cr	W	Mo	V	Al								
Plain Carbon	St.4	0.28	0.64	0.25	—	—	—	—	—	—	As rolled	50.2	32.6	27.1	27.8	58.4	153	8.5
Do.	St.5	0.36	0.53	0.19	—	—	—	—	—	—	do.	54.5	32.7	24.4	24.8	52.4	156	6.4
Cr-Si	ZX4C	0.36 0.45	— 0.4	1.2 1.6	— —	1.3 1.6	— —	— —	— —	— —	O.Q. 880° O.T 550°	93.5	82.8	78.8	12.7	57.6	240	7.8
Cr-Si-Mn	ZI179	0.32	1.08	1.04	0.21	0.93	—	—	—	—	O.Q. 880° A.T. 600°	85.4	71.8	61.8	14.8	65.9	231	9.4
Mn-Si-Mo	IZ	0.37	1.93	1.47	—	—	—	0.35	—	—	O.T. 680° O.Q. 860, T 550° O.Q. 860° T 300°	79.8 109.4 157.8	68.4 98.6 135.0	48.5 70.0 81.4	16.1 9.8 5.8	60.8 48.6 48.1	220 300 380	8.2 5.0 1.95
Cr-Mo	ZOXMA	0.23	—	—	—	0.93	—	0.26	—	—	O.Q. 880° O.T. 600°	84.0	74.0	73.3	11.5	65.0	220	15.3
	ZOXMHA	0.33	0.42	0.3	0.35	1.62	—	0.58	—	1.21	A.Q. 950° F.T. 650°	79.5	63.2	60.6	15.0	64.2	230	17.0
Cr-Ni	Z10	0.44	—	—	3.31	1.38	—	—	—	—	O.Q. 950° A.T. 575°	105.0	98.5	96.6	9.9	52.7	320	6.4
Cr-V	ZXTB	0.44	0.59	0.36	0.34	0.88	—	—	0.2	—	O.Q. 880° A.T. 600°	67.2	36.0	34.9	21.4	54.0	180	3.8
Cr-Mo-V	ZI10	0.24	0.50	0.31	0.15	1.70	—	0.25	0.30	—	O.Q. 880° O.T. 650°	116.7	106.6	101.7	7.5	54.7	335	15.7
Cr-Mo-V	Z5XMF	0.44	0.40	0.27	—	1.40	—	0.46	0.26	—	O.Q. 880° O.T. 650°	88.7	80.0	79.3	10.5	62.7	330	12.1
Cr-Ni-W	Z18	0.21	—	—	3.61	1.28	1.08	—	—	—	O.Q. 850° O.T 575°	91.1	77.8	75.1	18.6	68.0	290	14.6
Cr-Ni-V	Z14	0.21	0.35	0.25	3.96	1.06	—	—	0.29	—	O.Q. 850° O.T 580°	89.5	74.0	65.7	14.7	63.6	246	5.3
Cr-Ni-W	Z18	0.22	0.34	0.37	4.27	1.51	—	0.34	—	—	O.Q. 850° F.T. 650°	106.0	95.3	91.1	10.2	63.3	280	14.2
Cr-Ni-W	ZI84	0.38	0.45	0.25	1.43	0.72	—	0.22	—	—	O.Q. 850° A.T. 580°	71.1	37.3	36.1	17.0	39.1	194	4.5
Cr-Ni-W	Z5XHM	0.65	—	—	1.59	0.71	—	0.25	—	—	O.Q. 820° O.T. 600°	108.2	104.3	101.5	9.5	52.2	230	13.6
Cr-Ni-W	Z20	0.42	0.37	0.30	4.33	0.70	—	1.04	—	—	O.Q. 1,000° F.T. 190° O.T. 625°	111.5	60.0	34.7	9.2	33.2	—	6.2

KEY :—O.Q. = Oil Quench ; A.Q. = Air Quench ; T = Tempering ; O.T. = Tempering and cooling in oil ; F.T. = Tempering and cooling in furnace ; A.T. = Tempering and cooling in air.

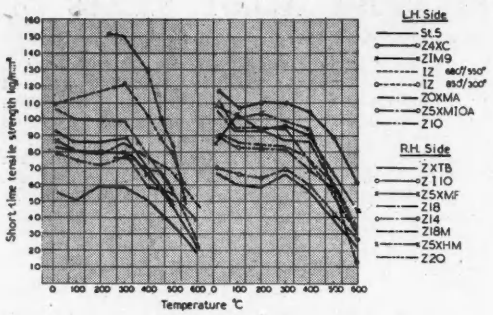

Fig. 1. **Variation in short-time tensile strength with temperature.**

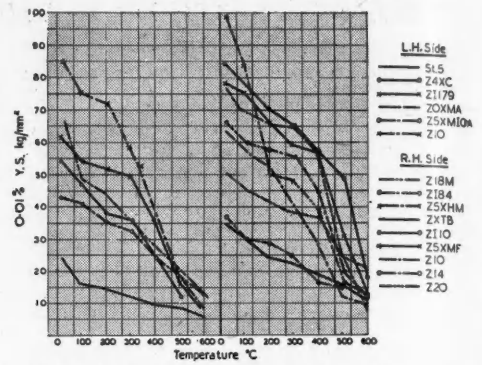

Fig. 2. **Variation in 0.01 per cent Y.S. with temperature.**

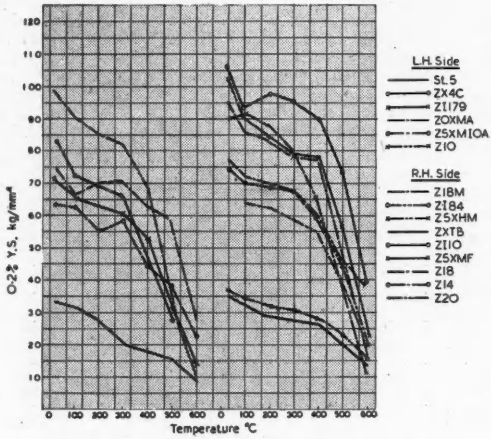

Fig. 3. **Variation in 0.2 per cent Y.S. temperature.**

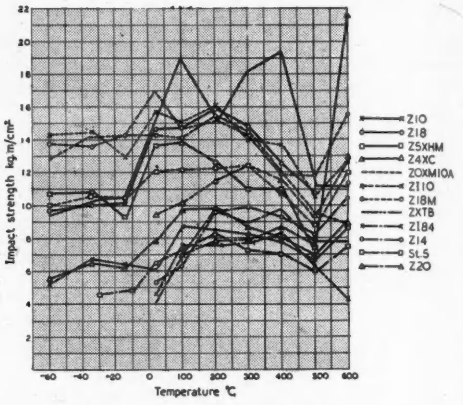

Fig. 4. **Variation in impact strength with temperature.**

strength at higher temperatures, which is to say, they certainly possess greater thermal stability.

The chrome-nickel steel Z10 possesses a very high short-time tensile strength up to 400 deg. C, but beyond this temperature it falls sharply; at 600 deg. C is approximates to that of plain carbon steel.

The Cr-V steel ZXTB possesses a lower short-time tensile strength over the entire temperature interval considered; while the Cr-Mo-V materials ZI10 and Z5XMF display higher short-time tensile strength up to 600 deg. C. The addition of 1.08 per cent tungsten as alloying material to Cr-Ni steel greatly increases the short-time tensile strength in the temperature range of 400-600 deg. C. The addition of tungsten to Cr-Ni must therefore be considered to affect very favourably the thermal stability of this material. Vanadium in amounts of 0.29 per cent, added to the Cr-Ni steel ZI4 increases but little the ductility in short-time rupture. But molybdenum additions to Cr-Ni steel increase the ductility of the material at elevated temperatures above 500 deg. C; and the large molybdenum percentage added to steel Z20 is therefore responsible for the increased short-time tensile strength displayed by this material in the temperature range of 500-600 deg. C. It is known that the 0.01 per cent and 0.2 per cent Y.S. values serve well to characterize the deformability of steel at elevated temperature, and they can therefore be employed as a standard of comparison for steels to be used for high temperature service.

Referring to Fig. 2, it will be seen that steel St.5 possesses the lowest 0.01 per cent Y.S. at temperatures ranging from 20 to 500 deg. C. At 600 deg. C, steel St.5, Z10 and ZI179 exhibit identical 0.01 per cent Y.S. values. In the temperature range of 20-500 deg. C the steels ZXTB and ZI84 also display low 0.01 per cent Y.S. values; but at 600 deg. C. the 0.01 per cent Y.S. value of these steels is approximately 1.7 times greater than that of the plain carbon steel. Steel ZI10 displays the highest 0.01 per cent Y.S. over the entire temperature range, although the steels Z5XMF, Z5XHM and Z18M also possess high 0.01 per cent Y.S. at 500 deg. C. Referring to Fig. 2, it will, however, be seen that the 0.01 per cent Y.S. of steel ZI10 tends to drop off as the temperature of 500 deg. C. is approached.

Referring to Fig. 3, it is seen that at 600 deg. C the steel Z5XMF possesses the highest 0.2 per cent Y.P. of the materials considered. The steels ZOXMA and ZOXM10A display relatively high Y.S. values over the entire temperature range considered, while steel Z20 possesses a comparatively low 0.01 per cent Y.S. value at 400 deg. C, but shows very high values at 500 deg. C, and especially at 600 deg. C. This fact again serves as proof of the beneficial effect of molybdenum upon the high temperature stability of alloyed steels.

The impact strength of all the materials tested proved to be sufficiently high at elevated temperatures. In fact it was in no case less than 6 kg. per sq. cm. Charpy. The impact strength of all steels examined is seen to increase as the temperature is raised to 300-400 deg. C. (Fig. 4). At 500 deg. C. the impact strength is

TABLE II. Creep of Steels under 12 kg./sq. mm. Stress at 475 deg. C.

Steel No.	St.5	ZI179	ZOXMA	Z5XM10A	Z10	ZXTB	ZI10	Z5XMF	Z18	Z14	Z18M	ZI84	Z5XHM	Z20
Permanent deformation after 200 hrs., % ..	0.81	0.39	0.017	0.0494	1.03	0.155	0.0098	0.0669	0.094	0.091	0.049	0.135	0.106	0.16
Creep rate during 100-200th hrs., %	83×10^{-5}	97×10^{-5}	5×10^{-5}	98×10^{-5}	225×10^{-5}	25×10^{-5}	7×10^{-5}	3×10^{-5}	30×10^{-5}	14×10^{-5}	20×10^{-5}	16×10^{-5}	17×10^{-5}	2×10^{-5}

seen to attain a minimum, but it rises again as the temperature is further increased, excepting steel ZI84.

The creep properties of the various steels were compared on the basis of a tensile stress of 12 kg. per sq. mm. at 475 deg. C. The data obtained are listed in Table II., where it is seen that the steels Z20, Z_1I10, Z5XMF, and ZOXMA possess very high creep strength. The materials Z10, ZI179, ZXTB, and steel St.5 are seen to have insufficient creep strength at 475 deg. C. With regard to the phenomenon of temperature brittleness, it is known from numerous investigations that this depends exclusively upon the temperature and not upon the stress to which the material is subjected, provided the stress is not so high as to produce a considerable amount of plastic deformation. In view of this fact the embrittlement tests were carried out on unstressed specimens. In order to reproduce the service conditions to which bolting materials are subjected in practice, the specimens were exposed to cyclic heating and cooling, about 80 thermal cycles being applied to the material. After the material had gone through heating and cooling cycles for 1,000 hours, the embrittlement was ascertained on the hot material by means of the Charpy test.

The steels ZI179, Z18 and Z14 were found to be subject to embrittlement. Steel Z10 displayed a loss of 30 per cent in impact strength after prolonged heating at 325 deg. C, but heating at higher temperature proved to raise its impact strength considerably above its initial value. This increase in impact strength was attended by a decrease in hardness. The steels ZOXMA, ZOXMIOA, ZXTB, ZI10, Z5XMF, Z18M ZI84, Z5XHM and Z20 proved to maintain their initial ductility. The temperature ranges within which the various materials were found to retain their initial hardness are listed in Table III. Referring to Table III, it will be seen that prolonged heating had no effect upon the steels containing nolybdenum or vanadium, or both molybdenum and vanadium.

Summarising the results of the various tests, it can be concluded that the steels ZI10 and Z20 are particularly suitable for operation under high stress at temperatures of 450 to 550 deg. C, while the steels ZOXMA, Z5XMF and Z18M may be used where a temperature range of 350-550 deg. C is concerned. The mechanical properties of the steels Z5X1M, Z18 and Z5XMIOA are satisfactory, but the steels ZOXMA, Z5XMF and Z18M are preferable because they are more resistant to temperature embrittlement.

TABLE III.

Steel No.	(*a*) Tempering temperature °C.	(*b*) Temperature limit to maintain original hardness, °C.	(*c*) Temperature margin between (*a*) and (*b*).
ZX4C	550	325	225
ZI179	600	400	200
30XMA	600	550	50
Z5XM10A	650	550	100
Z10	575	325	250
ZXTB	600	475	125
ZI10	650	475	175
Z5XMF	650	475	175
Z18	575	325	250
Z14	560	475	100
Z18M	650	475	175
ZI84	580	475	100
Z5XHM	600	475	125
Z20	625	550	75

APPLICATION OF X-RAY ANALYSIS OF METALLURGICAL PROBLEMS

By M. PAIC. (From *Revue de Metallurgie*, Vol. 41, July, 1944, pp. 169-179).

THE fact that X-rays are absorbed by matter provides a useful means for determining the chemical heterogeneity of alloys. The underlying principle of this method may be briefly described as follows: If a beam of X-rays of say 0.2 Å wave length passes through a sheet of aluminium of 1 cm. thickness, its intensity upon passage through the sheet will have decreased by 50 per cent as compared to its original intensity. If this weakened beam is subsequently passed through another aluminium sheet of the same thickness as the first, the intensity of the beam will decrease to 25 per cent of its original value, and so on. Thus a passage of the beam through a 10 cm. thickness of aluminium will decrease the intensity of the beam to 0.19 per cent of its original value; or, in other words, a ten-fold increase in the thickness of the penetrated aluminium sheet reduces the intensity of the beam to 1/263 of its original value. This reduction in the intensity of radiation is still larger, if copper is used in the place of aluminium, a copper sheet of 1 cm. thickness reducing the beam intensity to less than 0.01 per cent of its initial value.

This absorption of X-rays is a specifically atomic characteristic, one atom absorbing the same quantity of radiation regardless of whether the matter concerned is in the solid, liquid, or gaseous phase, and whether or not it is combined with other elements. The way in which the X-ray absorption of the 92 elements varies, is shown in Fig. 1, where it is seen that for a given thickness of crystallised elements the absorption does not vary in direct proportionality with the atomic number, but passes in regular manner through subsequent maxima and minima in accordance with the system of periodicity established by Mendeleeff. This curve, for example, shows that magnesium has a smaller absorbing power than aluminium, that copper is much more absorbent than aluminium, and so forth.

It will be readily understood that in a plate consisting

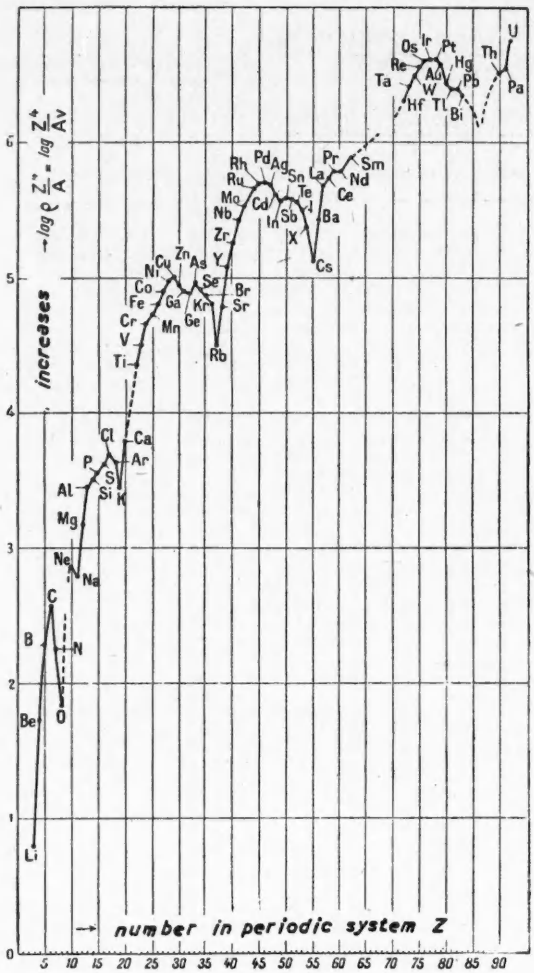
→ log ρ Z²/A = log Z²/Av
increases
→ number in periodic system Z
0 1 2 3 4 5 6
5 10 15 20 25 30 35 40 45 50 55 60 65 70 75 80 85 90
Li Be B C N O Ne Na Mg Al Si P S Cl K Ca Ar Ti V Cr Mn Fe Co Ni Cu Zn Ga Ge As Se Br Kr Rb Sr Y Zr Nb Mo Ru Rh Pd Ag Cd In Sn Sb Te I X Ba La Ce Pr Nd Sm Ta W Re Os Ir Pt Au Hg Tl Pb Bi Hf Th Pa U

Fig. 1. Absorption of X-rays by various elements arranged in the order of the periodic system, with the absorption based on the function $\left(S\frac{Z^4}{A}\right)$ where A = atomic weight, ρ = spec. gravity, and Z = atomic number.

of an alloy of aluminium and copper the X-rays will suffer greater absorptions in the parts which are richer in copper, and lesser absorptions where the aluminium content prevails. This phenomena can be utilised to study the segregation in castings, as exemplified by Fig. 2, which shows the X-ray picture of an aluminium billet containing 2.24 per cent lead. Here the segregation of the lead is seen to be particularly intense. At the solidification temperature of the aluminium the liquid lead is not miscible with the aluminium, and it therefore coalesces in droplets which prior to the solidification of the aluminium descent to the bottom of the billet; hence the dark region at the bottom of the radiograph.

With the photo-electric method the varying degree of blackness of the radiograph can be measured and indicated by means of a galvanometer. By slicing a test piece into thin plates and subjecting each one of these to X-ray analysis this relative composition can therefore be obtained, as exemplified by Fig. 3. In this graph the copper percentages of the alloy are determined on the basis of the experimentally established per cent Cu *vs* degree of blackness diagram shown in the right hand part of the graph.

Fig. 2. Lead segration in aluminium ingot of 70 mm. dia. with 2·24% lead content.

This "radio analytical" method is applicable to all binary alloys, provided that the two constituents have different characteristics of X-ray absorption. It may be objected that more often than not commercial aluminium alloys are not of binary nature, but are far more complex. It therefore remains to be shown that this method is also applicable to complex alloys such as e.g., duraluminium, which contains magnesium, manganese, silicon, and iron, in addition to aluminium and copper. Referring to Fig. 1, it will be seen that while manganese and iron are less absorbent to X-rays than copper, they are much more absorbent than aluminium. Silicon is seen to closely approach the absorbed power of aluminium, while magnesium absorbs a little less than aluminium. Therefore, the absorption of X-rays effected by duraluminium will be slightly larger than that of an aluminium-copper alloy which contains the same amount of copper as the duraluminium. Vice versa, an aluminium-copper alloy absorbing exactly the same amount of X-ray radiation will have a slightly larger copper content than duraluminium. The copper content of an aluminium-copper alloy which shows the same X-rays absorption as duraluminium may therefore be used to characterise the composition of the duraluminium. This copper content may be termed "the copper index" of the duraluminium.

Thus the radio-analytical method permits to determine the copper index at each point of a duraluminium sheet. If, for example, at one point a copper index of 5.5 is found, this will mean that at this point the absorbing power of the sheet is equivalent to that of an aluminium-copper alloy containing 5.5 per cent copper. The determination of the copper index is carried out in the same way as that of the aluminium-copper alloy. The results of such a determination are charted in Fig. 3, which shows the inequality of the copper index of a duraluminium sheet. It may be added that the application of this radio-analytical method is not limited to alloys, but may also be applied to liquids. The aforementioned study was carried out at the research department of the Compagnie des Produits Chimiques et Electrometallurgiques Alais, Froges et Camargue at Chambéry, Savoy, France.

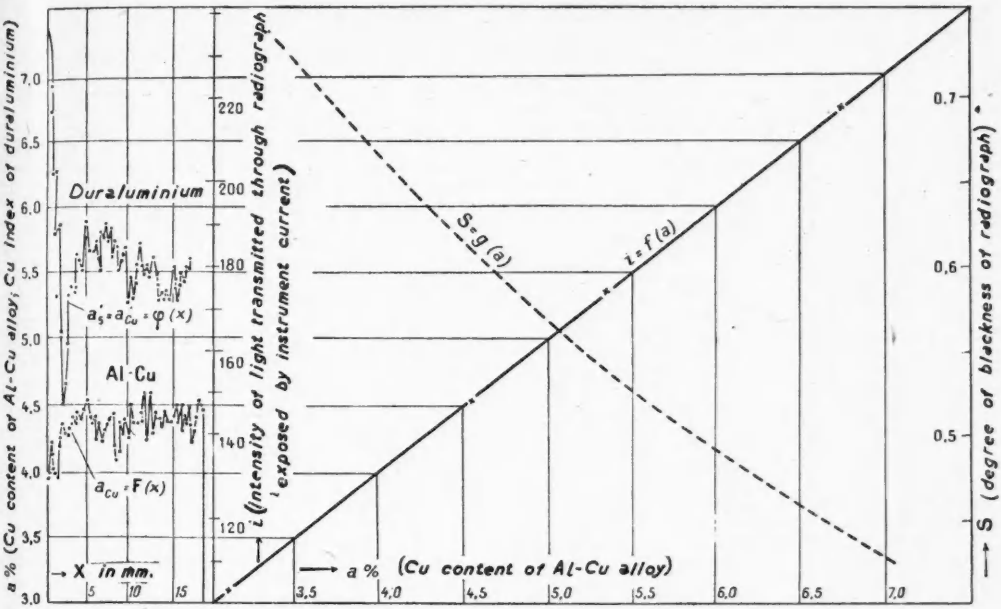
a % (Cu content of Al-Cu alloy; Cu index of duraluminium)
Duraluminium
Al-Cu
$a_s = a_{Cu} = \varphi(x)$
$a_{Cu} = F(x)$
i (intensity of light transmitted through radiograph exposed by instrument current)
S = g(a)
z = f(a)
→ X in mm.
→ a % (Cu content of Al-Cu alloy)
→ S (degree of blackness of radiograph)

Fig. 3. **Determination of metal homogenity by photometric evaluation of the X-ray pictures.**

CHROME PLATING INCREASES LIFE OF FORGE DIES

(From *Z.d.V.D.I.*, February, 1945, pp. 67-68).

THE life of forge dies can be increased successfully by chrome plating. The process can be applied to dies for light to medium-weight forgings with various, except vary deep, engravings. In the case of dies with very deep engravings, it will be of advantage to apply chrome plating at least to those parts of the surface which are in the path of the overflowing material, as by this means the wear caused by the latter will be reduced considerably.

Good results were obtained by chrome plating the die used for making the forging shown in Fig. 1. The average life before plating was 15,000 forgings and this was increased to 35,000 by the plating. Still better results were obtained with dies for the production of forged spanners and gas tongs (Fig. 2). The dies used for the latter are subjected to the heaviest wear at the point marked X, which must therefore be re-plated as soon as the chromium layer is worn down.

By plating the pin of the die for forging the part shown in Fig. 3 the life of the die was increased from between 1,500 and 2,000, to from 8,000 to 10,000.

Before the dies are plated they must be thoroughly tested under the hammer to enable possible faults to be detected and corrected. Thereafter the surfaces, edges and engravings to be plated must be highly polished, as otherwise subsequent touching-up may be necessary which may cause the advantages of the chromium plating to be lost.

The increase of the life mentioned due to chromium plating is always possible with dies made of ordinary steel, but it is not always possible with dies made of special steel. The thickness of the chromium layer must not exceed 0.03 mm, as this would make it too brittle, particularly if temperatures of over 100 deg. C. are reached and if the thermal expansion of layer and base metal differ.

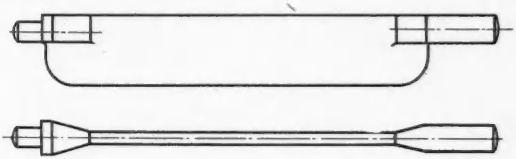

Fig. 1.

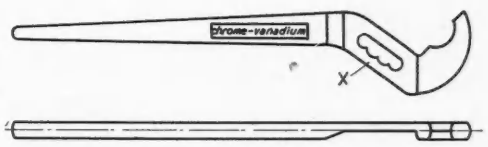

Fig. 2.

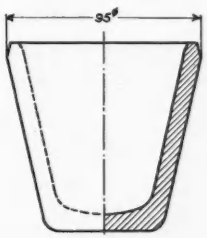

Fig. 3.

SOME APPLICATIONS OF HYDRAULIC MOTORS

By C. F. JACOBSON. (From *Teknisk Tidskrift*, Vol. 75, February 17th, 1945, pp. 179-183).

HYDRAULIC motors are employed for certain engineering purposes, particularly where questions of speed control are involved or where a small actuating impulse must be transformed into a large control force. In addition to these well known applications, hydraulic motors are also employed in a number of industrial plants. Some cases are described below in which hydraulic *Imo-motors* are used in industry.

The *Imo-motor* consists of three jointly operating screws which are placed in a joint casing. A characteristic feature of this design is that the screw threads can be so dimensioned that the middle-screw, that is, the driven screw, performs all the work, while the two side-screws, or trailing screws, only serve as seals. In the design shown in Fig. 1, in which the screws are carried in axial ball bearings, the motor is reversible. It can operate in two directions of rotation, as the ball bearings take up the axial thrust caused by the pressure of the working fluid, i.e., of the oil, for which two alternative inlet connections are indicated in Fig. 1.

In Fig. 2 is shown an *Imo-motor* with oppositely threaded screw-halves. In this design, in which the axial thrust is completely balanced, the oil may be admitted at the centre so that it passes in double-flow through the motor. The discharge oil is passed out through a common discharge connection. Both the designs (Figs. 1 and 2) are seen to contain only three rotating parts which are dynamically balanced. The working medium is oil, a lubricating oil of suitable viscosity being usually employed. Where the motor is to operate at low temperature, a transformer oil or some special brand of oil is used.

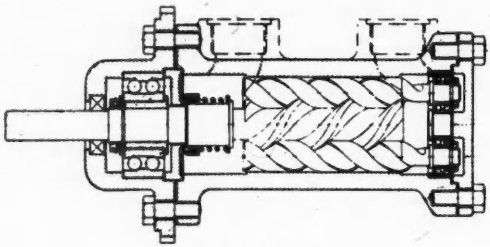

Fig. 1. **Reversible Imo-motors.**

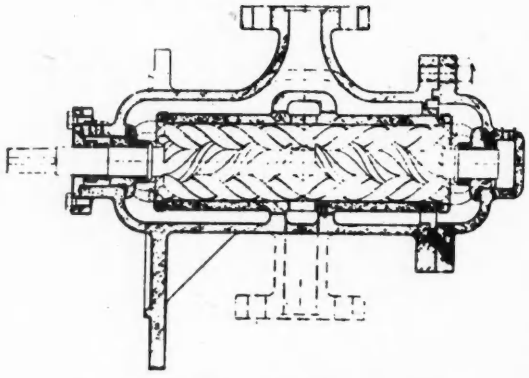

Fig. 2. **Reversible Imo-motor for double flow.**

The installation shown in Fig. 3 is typical of a plant in which the hydraulic drive is chosen because of danger of explosion. This particular plant, which serves for the manufacture of explosives, consists of four nitrate centrifugals driven by a 10 h.p. motor. The working process consists in filling the centrifugals with cellulose and nitric acid. The centrifugals are then set in motion and kept in operation at approx. 20 r.p.m. for a certain length of time. After that, the acid is drained off and the nitrate cellulose is desiccated by bringing the centrifugal up to a speed of 900 r.p.m. The working fluid, that is, pressure oil, is supplied to the motors through a piping system connecting with two oil pumps of different capacities. These pumps, which are driven by electric motors, are placed in a safe location not exposed to the danger of explosion.

Each *Imo-motor* has a manœuvering valve by which it can be connected either to the smaller or to the larger pump. If connected to the smaller pump, the centrifugal will run at 20 r.p.m., and if to the larger pump, at 900 r.p.m. The oil flow is so directed by the manœuvering valve that the centrifugal turns in clock-wise rotation when operating at low speed and in anti-clockwise rotation when running at high speed. Shutting down of the centrifugal is accomplished by bringing the manœuvering valve into the "stop" position. The motor will then operate as pump and will discharge pressure oil into the discharge line, braking being accomplished by means of a throttle valve which is combined with the manœuvering valve.

The plant circuit is so laid out that the motors operate in series. No motor can therefore receive more than a certain rate of oil, and the maximum speed cannot exceed 900 r.p.m. Furthermore, the plant is so dimensioned that, e.g., one centrifugal may operate at low speed, while two other machines run at high speed, the fourth centrifugal being at rest for the purpose of filling or emptying. This mode of operation is enforced by appropriate interlocking of the four manœuvering valves. For reasons of safety the manœuvering valves are placed at a considerable distance from the centrifugals.

The accelerating and braking characteristics of a centrifugal of this type are plotted in the diagram shown in Fig. 4. The acceleration characteristic is seen to be very smooth, full speed, which in this case is 850 r.p.m., being reached after 120 seconds. Moreover, the time required for acceleration may be adjusted by means of a by-pass valve; this is possible because system pressure and motor torque are in direct proportional relationship. The torque required is greatest at the moment of starting, and the oil pressure characteristic shows that this drops to the same extent as the speed of the centrifugal increases. The braking characteristic indicates that the centrifugal comes to rest within 80 seconds after bringing the valve in the "stop" position. A view of the *Imo-motor* and its manœuvering valve is given in Fig. 5.

The operating circuit of an aviation spirit plant equipped with Imo drives is shown in Fig. 6. In this case hydraulic drives were adopted because of the danger of fire and explosion. At the same time advantage was taken of the inherent facility of speed control offered by the hydraulic drive. This plant is equipped with two stirrers, five centrifugal pumps, one Imo-pump, and one vacuum pump, which are all fitted with individual Imo-drives. In this case series operation of the drives could not be resorted to, as the various hydraulic drives are of different sizes and are operated at different speeds. Each *Imo-motor* is therefore equipped for independent control, and all motors are

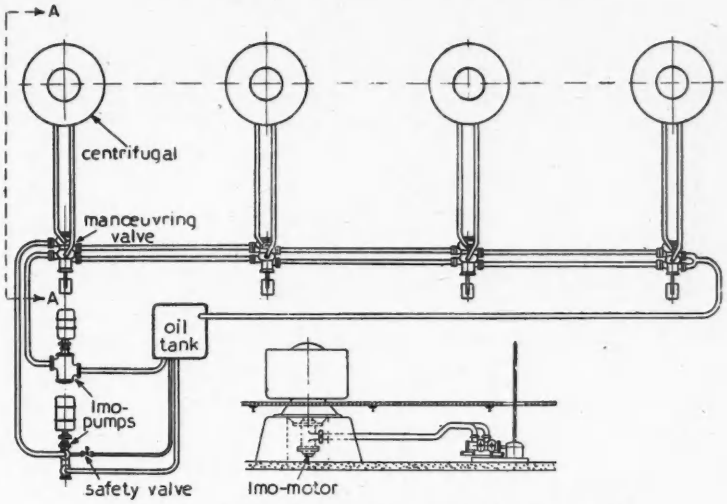

Fig. 3. **Centrifugals driven by Imo-motors in explosives plant.**

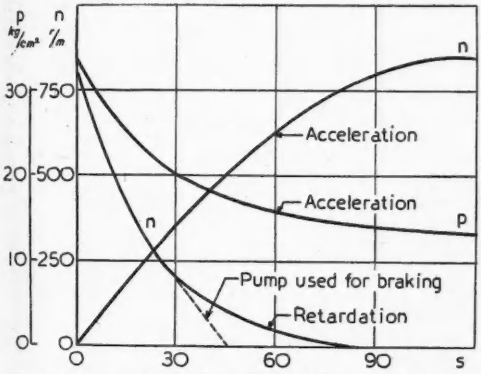

Fig. 4. **Characteristics of hydraulic drive for centrifugal.**

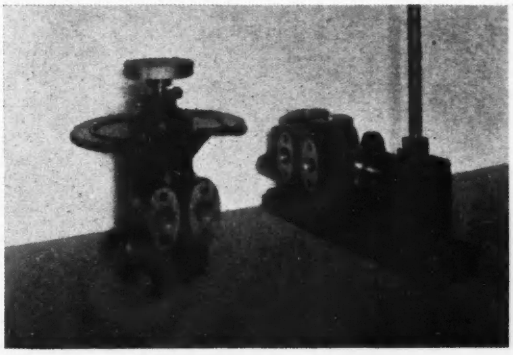

Fig. 5. **View of Imo-motor and manœuvering valve for centrifugal drive.**

operated in parallel from a common pressure mains and a return mains. The pressure mains is connected to the discharge of two Imo-pumps of different capacity. This enables the maintenance of three different rates of oil supply, according to whether one or the other, or both, pumps are in operation. Any pressure oil in excess of requirements is returned through a by-pass. The oil admission of each motor is equipped with a constant-supply valve, which is designed to pass a constant rate of flow irrespective of the motor load. It will be readily understood that if this valve were not provided and a motor were suddenly to lose its load, it would begin to race, thus robbing the other motors in the circuit of their oil supply. A view of a constant flow valve is given in Fig. 7.

A special type of *Imo-motor* is used to drive a mill for the rolling of metal foil (Fig. 8). This motor is actually a twin unit, with one unit placed on top of the other, both units and their direc-

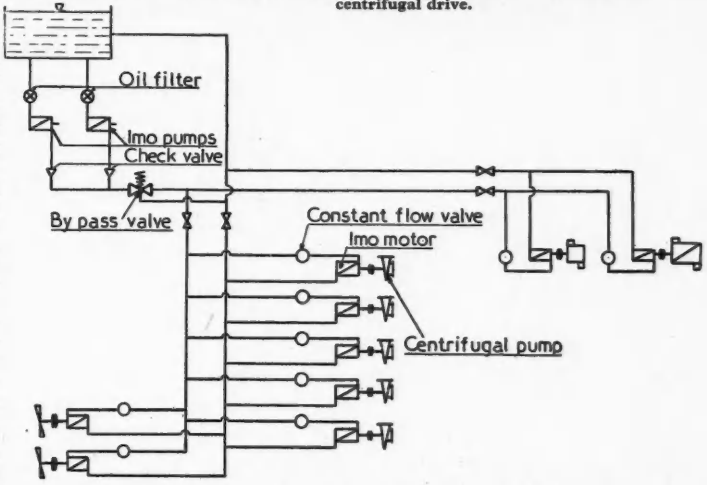

Fig. 6. **Hydraulic drives in chemical plant.**

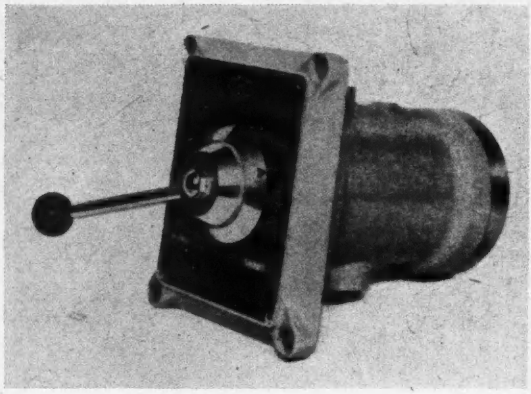

Fig. 7. **Constant flow valve.**

tion of rotation being controlled by a common valve. Each unit delivers 50 h.p. at 570 r.p.m. The vertical distance between the motorshafts is 140 mm.

This is also the distance between roll centres, thus enabling the direct coupling of the rolls with their respective drives. Remote control of the mill and its drives is provided; it is powered by a 0.4 h.p. electric motor placed on top of the hydraulic drive. There is also a magnetic brake for stopping the unit without loss of time. The importance of this measure may be gauged from the fact that the metal foil passes through the mill at a speed of 250 m. per minute. Moreover the foil is so thin that it easily crumples and breaks with careless handling. The small fly-wheel effect of the *Imo-motor* and the absence of a reduction gear and the consequent facility of quick manœuvering and reversing of the mill are therefore of particular advantage. The control circuit of this Imo drive is shown in Fig. 9. The pressure oil is seen to be supplied by an Imo-pump to the two motors *via* a control valve, the two motor units of the drive being arranged in series as far as the flow of the pressure oil is concerned. Identical speeds of the motors is therefore obtained without any mechanical coupling. This mode of operation imparts a certain flexibility to the operation of the rolls, which is of importance if the rolled material possesses surface irregularities or if the roll diameters are not absolutely identical.

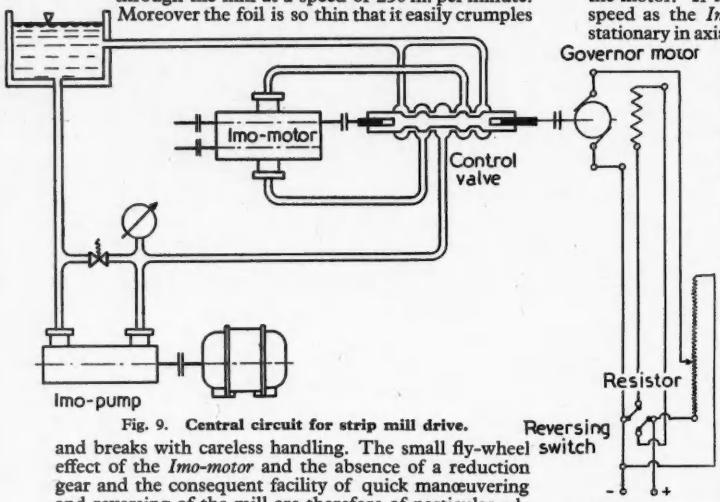

Fig. 9. **Central circuit for strip mill drive.**

The admission valve of the rotary piston type, which controls both speed and direction of rotation, is kept in permanent rotation during operation, hereby ensuring an easy shifting of the valve piston in axial direction. On one end the control valve piston is driven by a chain

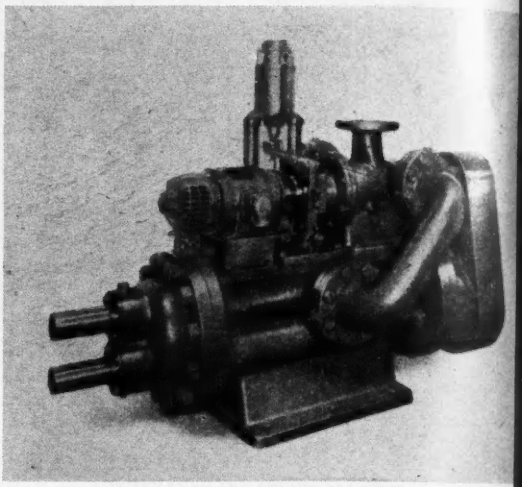

Fig. 8. **Hydraulic drive for strip mill.**

drive from one of the two *Imo-motors*, while its other end is coupled with the electric motor control drive by means of a threaded shaft which extends into a correspondingly threaded central bore of the valve piston. The electric motor comprising the control drive is of the shunt type, a controller being provided for adjusting the motor speed and reversing the direction of rotation of the motor. If this motor is adjusted to run at the same speed as the *Imo-motors*, the valve piston will remain stationary in axial direction, and the valve opening will remain unchanged. However, if the *Imo-motors* and the governing motor are running at different speeds, the difference in speed will cause the piston to travel in the one or the other direction along the threads of the shaft of the governing motor, and the valve opening will therefore change. This change in the valve opening in turn will change the rate of oil supply to the *Imo-motors*, and consequently their speed, until this again equals that of the governing motor. *Vice versa*, a change in the speed of the *Imo-motors* will be achieved by changing the speed of the governing motor.

Hydraulic motors can also be built for high speed operation, as exemplified by Fig. 10, which shows a unit capable of delivering 2 h.p. at 10,000 r.p.m. Motors of this type find application to grinding wheel spindles and for other purposes where drives of small dimensions and with small rotary masses are required.

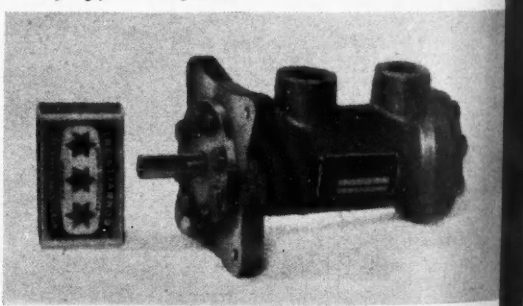

Fig. 10. **Imo-motor of 2 h.p. output at 10,000 r.p.m.**